THE JOURNAL OF PHYSICAL CHEMISTRY A
A JOURNAL OF THE AMERICAN CHEMICAL SOCIETY

pubs.acs.org/JPCA Article

Autodetachment over Broad Photon Energy Ranges in the Anion Photoelectron Spectra of $[O_2{-}M]^-$ (M = Glyoxal, Methylglyoxal, or Biacetyl) Complex Anions

Published as part of The Journal of Physical Chemistry virtual special issue "125 Years of The Journal of Physical Chemistry".

Marissa A. Dobulis, Conor J. McGee, Thomas Sommerfeld,* and Caroline Chick Jarrold*

Cite This: *J. Phys. Chem. A* 2021, 125, 9128–9142 Read Online

ACCESS | Metrics & More | Article Recommendations | Supporting Information

ABSTRACT: Complexes of anion–neutral pairs are prevalent in chemical and physical processes in the interstellar medium, the atmosphere, and biological systems, among others. However, bimolecular anionic species that cannot be described as simple ion–molecule complexes due to their competitive electron affinities have received less attention. In this study, the $[O_2{-}M]^-$ (M = glyoxal, methylglyoxal, or biacetyl) anion photoelectron spectra obtained with several different photon energies are reported and interpreted in the context of *ab initio* calculations. The spectra do not resemble the photoelectron spectra of M^- or O_2^- "solvated" by a neutral partner. Rather, all spectra are dominated by near-threshold autodetachment from what are likely transient dipole bound states of the *cis* conformers of the complex anions. Very low Franck–Condon overlap between the neutral $M{\cdot}O_2$ van der Waals clusters and the partial covalently bound complex anions results in low-intensity, broad direct detachment observed in the spectra. The $[O_2$-glyoxal$]^-$ spectra measured with 2.88 and 3.495 eV photon energies additionally exhibit features at ∼0.5 eV electron kinetic energy, which is more difficult to explain, though there are numerous quasibound states of the anion that may be involved. Overall, these features point to the inadequacy of describing the complex anions as simple ion–molecule complexes.

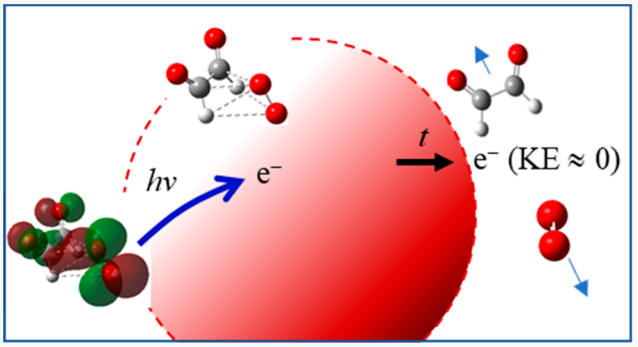

INTRODUCTION

Ion–molecule complexes (IMCs) are a class of systems that have long attracted interest because of their importance in gas-phase reactions and photochemistry,[1−9] the properties and dynamics of aqueous electrolytic solutions,[10−12] and physical processes in planetary atmospheres.[13−17] Our group recently reported on a series of studies on negatively charged ion–molecule complexes as precursors to atmospherically relevant neutral collision complexes formed between O_2 and several nonpolar and polar volatile organic complexes (VOCs).[18,19] These IMCs could be described, with one exception (VOC = formaldehyde), simply as $O_2^-{\cdot}$VOC. That is, the excess charge in the $O_2^-{\cdot}$VOC complexes was unambiguously localized in the π_g molecular orbital of O_2, and while the degeneracy of the π_g orbitals was broken, they remained very close in energy and separate from the VOC-local orbitals. This description comports with the fact that O_2 has a positive electron affinity (EA) while the VOC partners in the study have negative EAs.

In a related study, evidence of charge transfer to temporary anion states in the $O_2^-{\cdot}C_6H_{6-x}F_x$ ($0 \le x \le 5$) IMCs was observed.[20] The anion photoelectron (PE) spectra of these IMCs exhibited significant PE signal enhancements at electron kinetic energies corresponding to the $C_6H_{6-x}F_x^-$ temporary anion states, meaning that a charge transfer to fleeting $O_2{\cdot}C_6H_{6-x}F_x^-$ states was affected via photoexcitation, in competition with direct detachment. In addition to the temporary anion states, several of the IMCs exhibited unexpected nonvalence bound anion states, the evidence for which was the distinct vibrational autodetachment signal observed near the zero-electron kinetic energy limit of the spectra. This signal was unexpected because neither of the neutral molecules in the complex has physical properties (e.g., they lack exceptionally high polarizability and large dipole or quadrupole moments) that would support a nonvalence-bound anion state.

Received: August 12, 2021
Revised: September 25, 2021
Published: October 8, 2021

https://doi.org/10.1021/acs.jpca.1c07163
J. Phys. Chem. A 2021, 125, 9128–9142

Another thought-provoking feature of this series of $O_2 \cdot C_6H_{6-x}F_x^-$ IMCs was the evolution of the EAs across the series of free $C_6H_{6-x}F_x$ molecules, which were predicted by Driver and Jena[21] to smoothly transition from approximately −1 eV (i.e., the anion is unstable with respect to the neutral) to approximately +1 eV as x increases from 0 to 6. They calculated the EA of tetrafluorobenzene to be nearly zero, with pentafluorobenzene predicted to have an EA comparable to that of O_2. Describing the anion of the $O_2 \cdot C_6HF_5$ complex within a simple IMC framework was therefore of questionable utility, although the PE spectrum of the complex suggested that $O_2^- \cdot C_6HF_5$ was a reasonable description. We also reported the PE spectrum of the anion of $O_2 \cdot C_6F_6$, which was strikingly different from the spectra of the less-fluorinated species in terms of EA and the Franck−Condon profile of the detachment transition, inconsistent with either the $O_2^- \cdot C_6F_6$ or $C_6F_6^- \cdot O_2$ description. This observation suggested that the anion might have covalent or partial covalent bonding between O_2 and C_6F_6, whereas the most stable form of the neutral would be a simple van der Waals complex.

Here, we present new results of an anion PE spectroscopic study of $[O_2{-}\boldsymbol{M}]^-$ ($\boldsymbol{M}$ = glyoxal, methylglyoxal, dimethylglyoxal, or biacetyl) bimolecular complex anions in which both partners have positive EAs and the associated neutrals form van der Waals complexes. The anion PE spectra of glyoxal and the two methyl-substituted analogs have been previously reported by Sanov and co-workers,[22−24] who showed that all three have positive EAs higher than O_2. In descending order, the EA of glyoxal was reported to be 1.10 ± 0.02 eV,[22] methylglyoxal has an EA of 0.87 ± 0.02 eV,[23] biacetyl has an EA of 0.69 ± 0.02 eV,[24] and O_2 has an EA of 0.448 ± 0.006 eV.[25]

Along the glyoxal, methylglyoxal, and biacetyl series, the electron affinities decrease by approximately 0.4 eV while the triplet state (T_1) term energies increase slightly (2.38 eV, 2.41 and 2.46 eV, respectively).[26] The anions and the T_1 states share a common singly occupied molecular orbital (SOMO), which is the π_3 C−C bonding/C−O antibonding orbital. Both trends reflect how the increased electron "push" toward the C−C backbone by the methyl group(s) destabilizes the π_3 orbital.

All of the molecules in this study are chemically active in the atmosphere. Setting aside the perspicuous role of O_2, glyoxal is a tracer for the reaction pathways of biogenic compounds in the troposphere[27,28] as well as being a precursor to secondary organic aerosol formation[29,30] and has inspired a wide range of spectroscopic and theoretical studies.[31−39] Methylglyoxal is formed from the oxidation of diverse organic compounds in the troposphere[40−43] and its atmospheric interactions with glyoxal are of further interest,[44,45] while biacetyl is a ring-cleavage product in the NO_x oxidation of aromatics,[46,47] with implications for cloud chemistry.[48] These methylated analogs of glyoxal have also been the subject of spectroscopic examination.[49−55]

To set the stage for this current study, Figure 1 shows schematic potential energy curves (Leonard-Jones) for the (a) O_2 + *trans*-glyoxal and (b) O_2 *cis*-glyoxal bimolecular system based on the results of calculations (*vide infra*) and the close-lying anionic and neutral asymptotes. The neutral *cis*-glyoxal asymptotes lie 0.20 eV higher than the *trans*-glyoxal asymptotes, consistent with the experimental value of 0.21 eV determined by Parmenter and co-workers.[38] All asymptotes are set to experimental values, though the excited glyoxal anion state asymptote (dashed gray trace), which is indicated by an asterisk (*), is a short-lived, broad resonance.[52] The numerous states

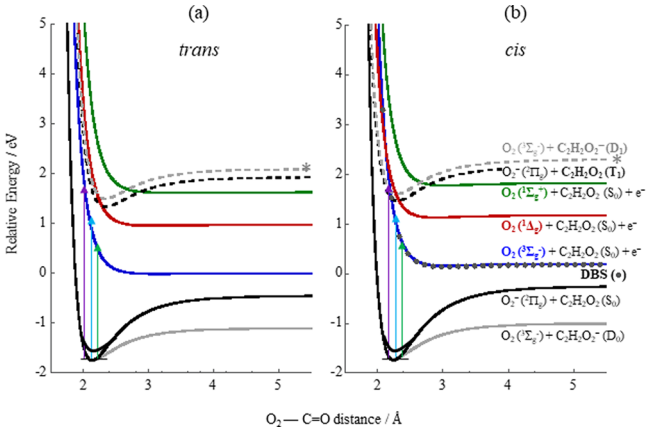

Figure 1. Leonard-Jones potential energy curves along the (a) *trans* and (b) *cis* conformers of the $[O_2$-glyoxal$]^-$ and O_2·glyoxal intermolecular distance coordinate. Solid black and gray traces correspond to the O_2^- ($^2\Pi_g$) + glyoxal (S_0) and O_2 ($X\ ^3\Sigma_g^-$) + glyoxal$^-$ (D_0) anionic limits, respectively, and dashed black and gray traces correspond to net anionic O_2^- ($^2\Pi_g$) + glyoxal (T_1) and O_2 ($X\ ^3\Sigma_g^-$) + glyoxal$^-$ (D_1) excited limits. The latter is marked with an asterisk (*). The temporary D_1 state of glyoxal$^-$ is a broad resonance, so a precise asymptotic energy is not available.[52] Colored curves correspond to van der Waals complexes associated with O_2 ($X\ ^3\Sigma_g^-$) + glyoxal (S_0) (blue), O_2 ($a\ ^1\Delta_g$) + glyoxal (red), and O_2 ($X\ ^1\Sigma_g^+$) + glyoxal (S_0) (green). The gray dotted curve in panel (b) represents a dipole bound state of the anion. (See the text.) Vertical arrows represent the 3.495 eV (purple), 2.883 eV (cyan), and 2.330 eV (green) photon energies used in this study.

arise from the close-lying electronic states of O_2 ($^3\Sigma_g^-$, $^1\Delta_g$, $^1\Sigma_g^+$), the low binding energies of O_2 (0.448 eV)[25] and glyoxal (1.10 eV),[22] the low-lying T_1 state of glyoxal (2.38 eV),[26] and a similarly low-lying excited doublet state (D_1) of the glyoxal anion. The lowest-lying excited neutral state would be the overall singlet O_2 ($^1\Delta_g$) + *trans*-glyoxal (S_0).[56]

The anion PE spectra of previously studied $O_2^- \cdot$VOC IMCs primarily exhibited a direct detachment signal having spectral Franck−Condon profiles like that of bare O_2^- but broadened and shifted to higher electron binding energy. This effect is due to the stabilization of O_2^- by the partner, in addition to Franck−Condon overlap between the IMC and the dissociative portion of the neutral O_2 − VOC potential.[18,19] It can be understood in the context of Figure 1, which shows the stability of the complex anion relative to isolated O_2^- + $\boldsymbol{M}$ (in the case of previously studied $O_2^- \cdot$VOC complexes, the O_2 − VOC$^-$ asymptote is not bound with respect to the neutral asymptotes). In contrast, the PE spectra of the $[O_2{-}\boldsymbol{M}]^-$ complex anions obtained using three photon energies (2.330, 2.881, and 3.495 eV) for $\boldsymbol{M}$ = glyoxal, methylglyoxal, or biacetyl are all dominated by intense, narrow signal with near-zero electron kinetic energy (e$^-$KE), regardless of the photon energy. This observation is inconsistent with direct detachment. Additional direct one- and two-photon detachment features are observed in the spectra as well. We consider the complex landscape associated with this series of complex anions, how to describe them appropriately, and how to understand their detachment transitions to two molecules that are not bound to each other except by van der Waals interactions.

METHODS

Experimental Section. The experimental PE imaging (PEI) apparatus has been previously described.[57] Glyoxal and methylglyoxal (each 40% wt in H_2O, Sigma-Aldrich) were dried

https://doi.org/10.1021/acs.jpca.1c07163
J. Phys. Chem. A 2021, 125, 9128−9142

using 3 Å molecular sieves for approximately 24 h prior to use and then heated; biacetyl (97%, Sigma-Aldrich) was used as is without any additional purification. A gas mixture of the trace organic of interest (glyoxal, methylglyoxal, or biacetyl), 30% O_2, and the balance being Ar was supersonically expanded into a vacuum chamber via a solenoid-type general valve (Parker series 9). A plasma was generated when the gas mixture expanded through an electrical discharge similar to that described by Duncan.[58] The resulting gas mixture was skimmed, and the anions were accelerated to 1 keV. The anions are then re-referenced to ground by a high-voltage potential switch[59] prior to passing into a Bakker-style time-of-flight mass spectrometer.[60,61] Anions of interest were selectively photodetached by the second (532 nm, 2.330 eV) and third (355 nm, 3.495 eV) harmonic outputs of a Nd:YAG laser (Continuum Surelite) or by the output of a pumped tunable optical parametric oscillator (Ekspla 240). Resulting photoelectrons were extracted using a velocity map imaging setup,[62] with images generated on a dual microchannel plate/phosphor screen recorded with a CCD camera using the NuACQ program provided by the Suits group.[63] Three-dimensional velocity distributions were obtained using the BASEX[64] program and then converted to e^-KE upon calibration based on the spectrum of O_2^-.[25] In general, PE spectra are plotted in terms of the electron binding energy (e^-BE) instead of e^-KE because e^-BE is photon-energy-independent (e^-BE = $h\nu - e^-$KE).

Using PEI as the method for kinetic energy analysis also provides the photoelectron angular distributions (PAD) associated with the detachment transitions. The nature of the orbital from which the electron is nominally detached governs the PAD. For randomly oriented molecular anions, the differential cross section is[65]

$$\frac{\partial\sigma}{\partial\Omega} = \frac{\sigma_{\text{total}}}{4\pi}\left[1 + \beta(E)\left(\frac{3}{2}\cos^2\theta - \frac{1}{2}\right)\right] \quad (1)$$

where $\beta = 0$ corresponds to an isotropic PAD, $\beta = 2$ corresponds to electrons ejected parallel to the electric field vector of the detachment laser, and $\beta = -1$ corresponds to electrons ejected perpendicular to the electric field. For atomic ions, there is a straightforward relationship between the angular momentum of the orbital involved in the detachment transition per Cooper and Zare.[65] For most polyatomic molecular anions, however, the relationship is more complicated, as angular momentum is no longer a good quantum number. Sanov has provided a cogent physical description that relates MOs to asymmetry parameters in molecular detachment transitions.[66] The asymmetry parameter, $\beta(E)$, is approximated using

$$\beta(E) = \frac{I_0 - I_{90}}{\frac{1}{2}I_0 + I_{90}} \quad (2)$$

where I_0 and I_{90} are the relative intensities of the electron signal distributed parallel and perpendicular to the electric field vector of the detachment laser. These values are calculated from images reconstructed using the pBASEX program.[67]

Theoretical. A broad survey of structures for all conformers of the $O_2 + \boldsymbol{M}$ ($\boldsymbol{M}$ = glyoxal, methylglyoxal, or biacetyl) anion and neutral complexes was conducted at the MP2/cc-pVDZ level using the *Gaussian 16* computational suite.[68] Possible speciation, such as adduct formation, including O_2 addition to the C centers, both with and without additional H-transfer, or O_2 insertion into a C−H bond, was also considered. For structures that converged, single-point calculations at the MP2/aug-cc-pVTZ level were completed. Time-dependent density function theory (TD-DFT) calculations were performed on the optimized MP2/cc-pVDZ anionic $\boldsymbol{M}$ molecules to get an approximate value for the $O_2 + \boldsymbol{M}^-$ (D_1) asymptote.

The MP2 survey was complemented by B3LYP/aug-cc-pVTZ and CAM-B3LYP/aug-cc-pVTZ calculations starting from the MP2 geometries. Results for relative energies from these density functional theory (DFT) methods were comparable to those obtained using the MP2 method, but intermolecular distances calculated with DFT were more comparable to orbital-optimized MP2[69] (OO-MP2, see below) optimized structures.

Structures and properties of the O_2-glyoxal complex anions were additionally investigated with OO-MP2 and coupled-cluster calculations. Specifically, coupled cluster with single and double substitution (CCSD) and noniterative triples (CCSD-(T)) and equation-of-motion CCSD (EOM-CCSD) were used. Both OO-MP2 and CCSD reduce spin-contamination prevalent for the studied species to negligible levels.

On the one hand, OO-MP2/def2-TZVPPD[70] optimizations and frequency computations were followed by CCSD(T)/aug-cc-pVTZ[71] single-point calculations. The frequencies show that all considered structures represent true minima on their respective potential energy surfaces and can be used to compute zero-point corrections (ZPC) for all adiabatic energy differences.

On the other hand, the ground states of the *cis* and *trans* conformers of the complex anions as well as their possible neutral and anionic fragments corresponding to *cis*- or *trans*-glyoxal and O_2 units were optimized with CCSD(T)/JUN-cc-pVTZ.[72] These optimizations enable us to estimate charge delocalization in the complex anions by comparing bond lengths in the complexes with their fragments.

In all coupled-cluster calculation, the 1s core electrons were frozen, and care was taken to check the largest T1 and T2 amplitudes to ascertain that none of the investigated species had significant multireference character.

The EOM-CCSD method was employed for two purposes. In the first place, dipole-bound states of *cis*-glyoxal and its associated *cis* conformer of the complex anion were characterized, and for this purpose, the AUG-cc-pVTZ set was augmented with a (7s7p4d) set of diffuse functions centered between the two H atoms. We note that the EOM-CCSD calculations also yield valence excited anion states, but for valence states, EOM-CCSD is expected to be less accurate than CCSD(T).

In the second place, stabilization calculations were carried out to investigate the D_1 state of the glyoxal anion.[73,74] In contrast to the bound D_0 state, the D_1 state represents a temporary anion, and our stabilization calculations yield the energy as well as the decay width Γ of the metastable state, which is related to its lifetime $\tau = \frac{\hbar}{\Gamma}$. For the stabilization calculations, the diffuse p function of the AUG-cc-pVTZ sets of all non-hydrogen atoms was augmented with an additional three diffuse p functions, and the exponents of these functions were scaled with factors of between 0.36 and 1.8.

The OO-MP2 and coupled cluster calculations were performed using version 4.2.1 of the ORCA[75] package as well as version 2.1 of the CFOUR package.[76]

RESULTS AND ANALYSIS

In the following section, the anion PE spectra of the $[O_2{-}\boldsymbol{M}]^-$ complex ions will be presented, followed by a survey of

https://doi.org/10.1021/acs.jpca.1c07163
J. Phys. Chem. A 2021, 125, 9128−9142

computed structures for the anions and neutrals. Focusing on $[O_2$-glyoxal$]^-$, we will characterize charge sharing or delocalization in the complex anion and consider the expected appearance of direct detachment to the van der Waals complex. We will then explore excited nonvalence and valence states of the anion that may be involved in the indirect autodetachment signal, and then we will consider other constitutional isomers that may contribute to spectroscopic features.

PE Spectra. The PE spectra of the ions with m/z corresponding to complexes formed between O_2 and glyoxal, methylglyoxal, and biacetyl (m/z 90, 104, and 118), respectively, are shown in Figure 2(a–c). The spectra were obtained using photon energies of 2.330 eV (532 nm, green traces), 2.883 eV (430.1 nm, blue traces), and 3.495 eV (355 nm, purple traces). Raw and reconstructed images are included in the Supporting Information. The spectra of all three anions, obtained with the three different photon energies, are dominated by intense signal at the highest e^-BE value accessible at each photon energy. That is, the most intense signal comes from electrons that are ejected with low e^-KE in a profile that looks similar in spectra measured at all three wavelengths. This type of signal is the hallmark of an indirect electron ejection process, such as thermionic emission or vibrational autodetachment.

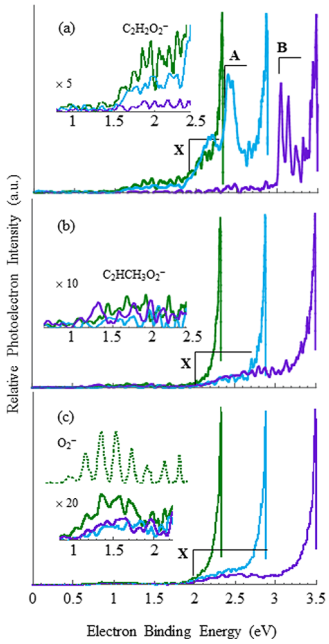

Figure 2. Anion PE spectra of the (a) $[O_2$-glyoxal$]^-$, (b) $[O_2$-methylglyoxal$]^-$, and (c) $[O_2$-biacetyl$]^-$ complexes obtained using photon energies of 2.330 eV (green), 2.883 eV (blue), and 3.495 eV (purple). All spectra are plotted in terms of e^-BE. The insets show a scaled signal that may be attributed to the direct detachment of (a) glyoxal, (b) methyl glyoxal, or (c) O_2^-, suggesting a two-photon process. Panel (c) also included the PE spectrum obtained for bare O_2^-.

These spectra bear no resemblance to the anion PE spectra of O_2^-·VOC IMCs published previously[18,19] (the spectrum of O_2^-·acetone is included in the Supporting Information for reference) which, as noted above, are described as being similar to the features in the PE spectrum of O_2^- shifted to higher e^-BE and broadened due to Franck–Condon overlap with the repulsive part of the neutral van der Waals potential. The indirect electron ejection signal evident in the spectra presented here will be addressed more thoroughly in the context of the theoretical results below. We first describe the other features in the PE spectra.

The spectrum of $[O_2$-glyoxal$]^-$ has a low-intensity, low S/N signal shown in the inset of Figure 2(a) that is consistent with the anion PE spectrum of the free glyoxal anion, while the PE spectrum of $[O_2$-biacetyl$]^-$ has a low-intensity signal consistent with the PE spectrum of bare O_2^-, which is shown in the inset of Figure 2(c). In both cases, the signal is more intense at the lowest photon energy. The signal shown in the inset of Figure 2(b) has a very poor signal-to-noise ratio but appears in the e^-BE range of the ground-state transition in the methylglyoxal anion PE spectrum.[23] In all three cases, this signal results from a two-photon process, where the first photodissociates the complex anion, forming either O_2^- + $\boldsymbol{M}$ or O_2 + $\boldsymbol{M}^-$, and the second photodetaches the daughter anion. As can be seen from the spectra, two photon processes make minor contributions to the spectra.

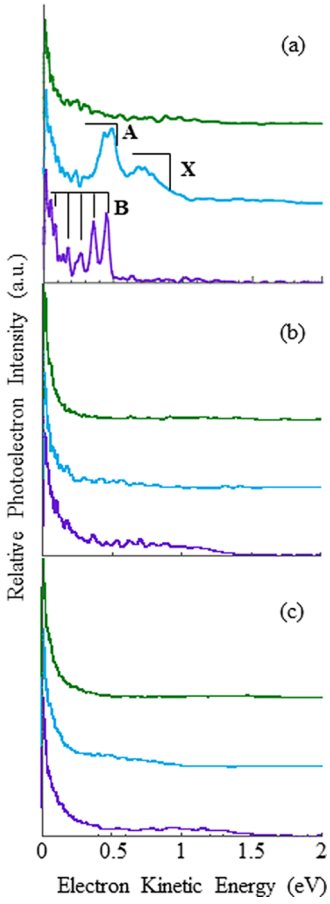

Figure 3. Anion PE spectra of the (a) $[O_2$-glyoxal$]^-$, (b) $[O_2$-methylglyoxal$]^-$, and (c) $[O_2$-biacetyl$]^-$ complexes obtained using photon energies of 2.330 eV (green), 2.883 eV (blue), and 3.495 eV (purple). All spectra are plotted against e^-KE. The vibrational progression of band **B** observed in the $[O_2$-glyoxal$]^-$ spectrum is highlighted with a comb in panel (a).

The anion PE spectra of $[O_2$-methylglyoxal$]^-$ [Figure 2(b)] and $[O_2$-biacetyl$]^-$ [Figure 2(c)] recorded at all three wavelengths are qualitatively very similar: both feature a broad, relatively low-intensity transition, labeled **X**, that appears to originate at approximately 2 eV, with vertical detachment energies (VDEs) at approximately 2.8 eV for $[O_2$-methylglyoxal$]^-$ and 2.5 eV for $[O_2$-biacetyl$]^-$ complexes. Because the

https://doi.org/10.1021/acs.jpca.1c07163
J. Phys. Chem. A 2021, 125, 9128–9142

transitions are so broad, the signal intensity (i.e., Franck–Condon overlap) at the origin may be nearly zero, making a more accurate determination of the EA difficult with this method; 2 eV should be considered to be an upper limit of the experimental EA of the neutral complex. This broad signal coincides in the spectra obtained with both 2.883 and 3.495 eV, consistent with direct detachment processes for both complexes. The 2.330 eV photon energy accesses only the rising edge of these transitions, and the spectra obtained with that photon energy is dominated by the indirect detachment signal near the threshold.

The spectrum of $[O_2\text{-glyoxal}]^-$ shown in Figure 2(a) exhibits additional features that distinguish this complex from the two methylated counterparts. In the spectra recorded with 2.330 and 2.883 eV, a broad signal labeled **X** overlaps with the high e^-BE tail of the glyoxal$^-$ direct detachment signal. The adiabatic detachment energy (ADE) is 1.9 ± 0.1 eV, and the VDE is 2.15 eV. In the 2.330 eV spectrum, this signal is part of a continuum between the glyoxal$^-$ direct detachment signal and the intense indirect detachment feature near the threshold. The spectrum obtained with 2.883 eV photon energy exhibits a distinct transition labeled **A** at 2.36 ± 0.05 eV, above the energy accessible with 2.330 eV photon energy. However, the spectrum measured with 3.495 eV reproducibly shows very little signal that is discernible from the noise that would coincide with **X** or **A**. Rather, a transition with a distinct 800 ± 15 cm^{-1} progression is observed with an origin of 3.05 ± 0.02 eV, labeled **B**. We note here the previously reported 801 cm^{-1} ν_6 out-of-plane C–H wag[77,78] vibrational mode of *trans*-glyoxal, and the C–C stretch in *cis*-glyoxal is 826 cm^{-1}.[79]

Other constitutional isomers of $C_2H_2O_4^-$, which would appear at the same m/z as $[O_2\text{-glyoxal}]^-$, will be considered further (*vide infra*), but we can immediately eliminate the possibility that oxalic acid is contributing to the spectrum based on the previously reported PE spectrum of the oxalic acid anion.[80]

Plotting the PE spectra against e^-KE provides additional insight, as shown in Figure 3(a–c). In particular, the profile of the near-threshold (e^-KE near-zero) features for the complexes do not appear to be photon-energy-dependent, though with methylation the profile of this signal is narrower. As illustrated in the Supporting Information, the signal does not follow a simple exponential decay nor is it consistent with thermionic emission from high vibrational levels of the anions. The widths of the signals at half-maxima are 0.067, 0.051, and 0.036 eV for $[O_2\text{-glyoxal}]^-$, $[O_2\text{-methylglyoxal}]^-$, and $[O_2\text{-biacetyl}]^-$, respectively.

Figure 3(a) shows that the signal associated with band **A** in the 2.883 eV PE spectrum and band **B** in the 3.495 eV PE spectrum of $[O_2\text{-glyoxal}]^-$ both appear at e^-KE values of approximately 0.5 eV. In addition, $[O_2\text{-glyoxal}]^-$ spectra obtained with small changes in photon energy over a 0.05 eV range near 2.883 eV, as shown in Figure 4, exhibit variations in the appearance of band **A** in the 2.883 eV photon energy spectrum. The red vertical line guides the eye along the e^-KE value, where the maximum intensity peak in band **B** appears in the 3.495 eV spectrum through the transitions labeled **A** in the spectra obtained with *ca.* 2.88 eV photon energy. The positions of these peaks have similar e^-KE values. Note also that the near-threshold autodetachment signal is unchanged but the profile and intensity of band **A** relative to the near-threshold signal vary. Similar spectra, with small variations in photon energy near 2.883 eV, are reported for $[O_2\text{-methylglyoxal}]^-$ and $[O_2\text{-biacetyl}]^-$ in the Supporting Information. No new features emerged in those spectra.

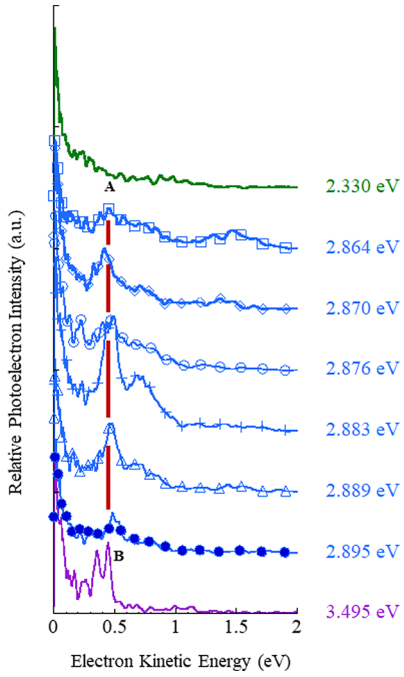

Figure 4. Anion PE spectra of $[O_2\text{-glyoxal}]^-$ plotted against e^-KE shown on an expanded scale. In addition to the spectra obtained with the three photon energies shown in Figure 3, additional spectra obtained in 50 cm^{-1} increments about the intermediate photon energy show that the relative intensity of band **A** [Figure 2(a)] appears to change relative to the intense feature near zero e^-KE, as shown by the vertical red line. The similarly obtained $[O_2\text{-methylglyoxal}]^-$ and $[O_2\text{-biacetyl}]^-$ spectra are reported in the Supporting Information and do not show variations in any features with photon energy.

PADs (included in the Supporting Information) provide an additional piece of information. In previous studies on $O_2^-\cdot$VOC complexes, the PADs were similar to the PE spectrum of O_2^-.[18,19,81] That is, for transitions with higher e^-KE, more electrons are ejected perpendicular to the electric field vector of the laser ($-1 \le \beta \le -0.5$), with the distribution becoming isotropic as e^-KE approaches zero. Glyoxal and methylglyoxal have also been previously shown by Sanov and co-workers to have small negative (perpendicular) anisotropy parameters.[22,23] In contrast, the signals in all three spectra shown here are isotropic. S/N is not sufficient to allow a precise determination of the asymmetry parameters, but they are close to zero. The PAD of electrons resulting from an indirect process, such as autodetachment, is typically isotropic since it is delayed relative to the initial photoexcitation.

We consider the possibility that the near-threshold features in the spectra may be autodetachment features. Autodetachment is typically observed in anion PE spectra when a valence or nonvalence bound state of the anion lies just below the detachment continuum, and vibrational excitation renders the anion unstable with respect to the loss of an electron. Autodetachment is therefore observed only when the photon energy is resonant with a transition to a quasibound vibronic level of the anion, and the resulting free electron carries away the excess energy between the intermediate excited anion and the final neutral vibronic level. Several examples of this effect are included in refs 82–94. In contrast with the more typical case of autodetachment, the near-threshold autodetachment signal is

https://doi.org/10.1021/acs.jpca.1c07163
J. Phys. Chem. A 2021, 125, 9128–9142

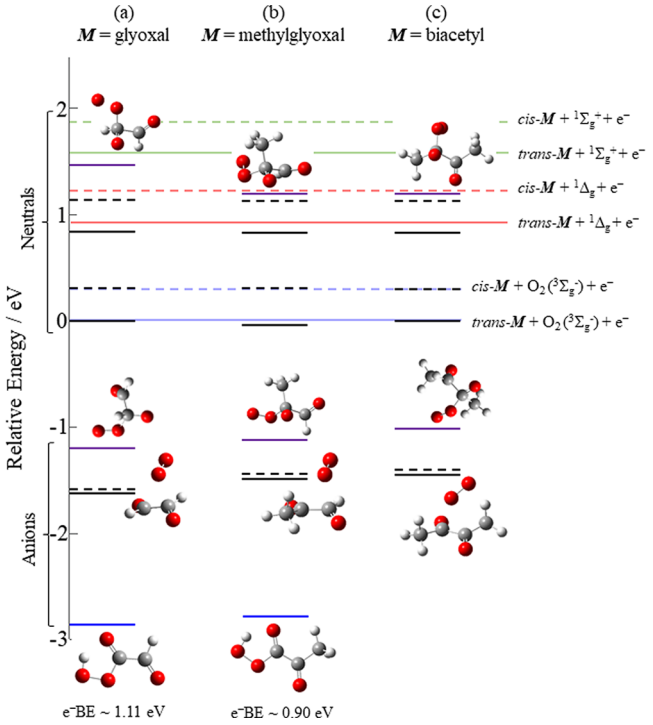

Figure 5. Summary of structures and relative energies of different species with m/z consistent with $[O_2{-}M]^-$; M = (a) glyoxal, (b) methylglyoxal, or (c) biacetyl along with their neutral counterparts, calculated at the MP2 level. Solid lines represent *trans* conformers, and dotted lines represent *cis* conformers. Black corresponds to the $[O_2{-}M]^-$ complex anions, dark-blue lines correspond to constitutional isomers formed by O_2 insertion into a C−H bond, and violet lines correspond to direct adducts with no additional bond rearrangement. The pale-blue, red, and green lines correspond to neutral glyoxal (S_0) + O_2 ($X\ ^3\Sigma_g^-$, a $^1\Delta_g$, B $^1\Sigma_g^+$) asymptotes, respectively.

observed over a range of photon energies for all three $[O_2{-}M]^-$ (M = glyoxal, methylglyoxal, or biacetyl) complexes. Specifically, this signal does not appear only at unique photon energies resonant with excitation to a quasibound vibrationally excited level of an excited state of the anion, the zero-point level of which lies below the detachment continuum. Computational results provide additional insights.

Computational Results. To determine the nature of the complex anions and to understand their detachment spectra with near-threshold autodetachment features, calculations on a wide range of anion and neutral complexes were completed. Possible speciation of the molecular complexes was also explored computationally. Covalently bound constitutional isomers could conceivably be associated with the narrower direct or indirect detachment features in the $[O_2$-glyoxal$]^-$ spectrum. Anionic and neutral structures included both the *cis* and *trans* conformers of M, the O_2 in different orientations relative to M, adducts, molecular structures that can be described as adducts with and without subsequent H-transfer, and C−H insertion products, many of which fell in the 3.495 eV energy window.

A pictorial summary of the main findings from the calculations run at the MP2 level is shown in Figure 5, with the energies of these complexes summarized in Table 1. (A comprehensive listing of the structures of the various anions and neutrals and their relative energies is included in the Supporting Information.) Energies indicated with solid lines in Figure 5 represent *trans*-M systems (optimized anion energies or neutral asymptotes), and dashed lines represent the *cis*-M analogs. The optimized structures that would be best described as IMCs in that both the O_2 and M remain intact and most closely resemble the separated molecules are predicted to be approximately 1.5 eV below the *trans*-M + O_2 ($^3\Sigma_g^-$) neutral asymptote (black lines), with relative stability decreasing modestly with methylation. This result is consistent with the backbone C centers becoming more electron-rich with methylation and also by the decrease in EA of the bare M (M = methylglyoxal or biacetyl).[22−24,23] The lower-energy constitutional isomers calculated for $[O_2$-glyoxal$]^-$ and $[O_2$-methylglyoxal$]^-$ anions are not consistent with the observed spectra as will be discussed further below.

We first describe results for the anionic complexes at approximately −1.5 eV relative to the neutral *trans*-M + O_2 ($^3\Sigma_g^-$) asymptote. At the MP2 level, charge is delocalized between O_2 and M; we therefore refer to these structures as $[O_2{-}M]^-$. A partial covalent bond is formed between an O atom

Table 1. Summary of Computationally Determined Relative Energies for the $[O_2{-}M]^-$ (M = Glyoxal, Methylglyoxal, or Biacetyl) Complexes and Neutral van der Waals Complexes Calculated at the MP2 Level

	M		
	glyoxal	methylglyoxal	biacetyl
	asymptote	**asymptote**	**asymptote**
neutrals	ADE/VDE (eV)	ADE/VDE (eV)	ADE/VDE (eV)
$O_2(^1\Delta_g)$ + *cis*-S_0	**2.97**	**3.00**	**3.00**
	2.91/3.38	2.86/3.36	2.86/3.33
$O_2(^1\Delta_g)$ + *trans*-S_0	**2.82**	**2.78**	**2.73**
	2.72/3.56	2.68/3.50	2.62/3.17
$O_2(^3\Sigma_g^-)$ + *cis*-S_0	**1.76**	**1.75**	**1.74**
	−/3.04	−/2.38	−/2.65
$O_2(^3\Sigma_g^-)$ + *trans*-S_0	**1.56**	**1.52**	**1.48**
	−/2.80	1.48/2.61	−/2.22
anions		**relative energy (eV)**	
trans-addition adduct	0.46	0.54	0.43
$[O_2$-*cis*$-M]^-$	0.002	0.06	0.06
$[O_2$-*trans*$-M]^-$	0	0	0
trans-C−OO−H insertion product	−1.31 (ADE = 1.09)	−1.17 (ADE = 0.89)	

https://doi.org/10.1021/acs.jpca.1c07163
J. Phys. Chem. A 2021, 125, 9128−9142

Table 2. Summary of the O_2-Glyoxal Single-Point and Zero-Point-Corrected Relative Energies Calculated Using CCSD(T)/aug-cc-pVTZ on Structures Optimized Using OO-MP2/def2-TZVPPD[a]

	E_{rel} (ZPC E_{rel})/eV	ADE/eV	VDE/eV
Neutrals			
cis-glyoxal···$O_2(^3\Sigma_g^-)$	0.201 (0.207)		
cis-glyoxal·$O_2(^3\Sigma_g^-)$	0.158 (0.227)	1.876 (1.866)	2.94
***trans*-glyoxal···$O_2(^3\Sigma_g^-)$**	**0.000 (0.000)**		
trans-glyoxal·$O_2(^3\Sigma_g^-)$	−0.019 (0.049)	1.712 (1.708)	2.84
Anions			
cis-glyoxal···$O_2^-(^2\Pi_u)$	−0.164		
trans-glyoxal···$O_2^-(^2\Pi_u)$	−0.365		
cis-glyoxal (D_0)···$O_2(^3\Sigma_g^-)$	−0.904 (−0.919)		
trans-glyoxal (D_0)···$O_2(^3\Sigma_g^-)$	−0.978 (−0.985)		
[O_2·*cis*-glyoxal]$^-$ (Q_1)	−0.940 (−0.911)		
[O_2·*trans*-glyoxal]$^-$ (Q_1)	−0.996 (−0.967)		
[O_2·*cis*-glyoxal]$^-$ (D_0)	−1.717 (−1.639)		
[O_2·*trans*-glyoxal]$^-$ (D_0)	−1.732 (−1.659)		

[a]Zero-point corrections shown in parentheses are from OO-MP2/def2-TZVPPD harmonic frequencies. Energies are set relative to the *trans*-glyoxal···O_2 ($^3\Sigma_g^-$) for comparison with Figure 1.

on O_2 and a C atom on ***M***. In the case of [O_2-methylglyoxal]$^-$, the partial O−C bond is formed with the more-electron-deficient C−H center rather than with the less-electron-deficient C−CH_3 center. The O_2−C internuclear distances in the [O_2-biacetyl]$^-$ anion are both ∼2.45 Å. The difference in energy between the *trans* and *cis* conformers of the complex anions (referring to the ***M*** family member) is very small, 0.06 eV or less, with the *trans* conformer being marginally more stable in all three ***M*** complex anions.

Higher-Level Calculations Characterizing the [O_2−Glyoxal]$^-$ Complex Anion. Focusing on the [O_2-glyoxal]$^-$ complex and neutral structures using OO-MP2/def2-TZVPPD followed by CCSD(T)/aug-cc-pVTZ single-point energy calculations, as summarized in Table 2, the complex anions are calculated to be more stable relative to their respective neutral dissociation asymptotes compared to the lower-level calculations. The EAs were calculated to be 1.66 eV for the *trans* conformer and 1.85 eV for the *cis* conformer. This difference in the binding energies of the *trans* and *cis* conformers is attributed to the two conformers of the anion lying within 0.02 eV, while the *cis* conformer of the neutral is less stable than the *trans* conformer by 0.2 eV.

For further optimization using the CCSD(T)/Jun-cc-pVTZ method, the O_2−C internuclear distance in the [O_2-glyoxal]$^-$ complex anion is predicted to be 2.26 Å for the *cis* conformer and 2.14 Å for the *trans* conformer; these values are reflected in Figure 1. The O_2−C internuclear distances calculated using CAM-B3LYP/aug-cc-pVTZ are similar to those calculated at the OO-MP2 level. These relatively short internuclear distances suggest a partial covalent bond formed through charge delocalization between the O_2 and glyoxal partners in the complex anion.

The extent of this charge delocalization in the complex anion was explored in several ways. First, natural bond orbitals (NBO) of the SCF density at the DFT-optimized structures of [O_2-glyoxal]$^-$ predict that the glyoxal portion of the complex carries a charge of −0.2. A second perspective is provided by the Mullikan and Loewdin populations derived from the OO-MP2 relaxed density. Both schemes suggest that in both [O_2-*cis*-glyoxal]$^-$ and [O_2-*trans*-glyoxal]$^-$ the spin density (the unpaired electron) resides entirely on the O_2 moiety while the excess charge is split 40:60 between the glyoxal and O_2 units. In other words, the doubly occupied π^* orbital on O_2^- donates electron density to the π_3 LUMO of glyoxal, while its singly occupied π^* orbital is oriented parallel to the glyoxal plane so that no direct interaction is possible.

A third option for analyzing the charge delocalization is to study bond-distance changes between the complex anions and their neutral and anionic fragments. For this purpose, structures of molecular O_2, glyoxal anions, and neutrals along with the complex anions were optimized with the CCSD(T)/JUN-cc-pVTZ method. The relevant calculated bond distances are summarized in Table 3 along with several experimental values.[25,56,95,96] We note that while the individual CCSD(T)/JUN-cc-pVTZ bond lengths agree with experiment reasonably well, trends will undoubtedly be far more reliable than any single value.

Specifically, we analyze three trends: the O−O bond of the O_2 or O_2^- units, the C−C bond length, and the formal C═O double bonds of glyoxal. With the exception of the [O_2-*trans*-glyoxal]$^-$ complex anion, the two CO bonds are symmetry-equivalent.

We start with the O_2 bond distance. The O_2 bond length in the complex anions lies between the respective isolated anion and neutral bond distances but is somewhat closer to the O_2^- anion, suggesting that more excess charge is carried by the O_2 unit. This conclusion is supported by the bond lengths in the glyoxal subsystems. In particular, the C−C distances in the complex anions are very close to those of neutral glyoxal, and the CO lengths lie between the neutral and anionic values but are somewhat closer to the neutral distances. Thus, the bond length analysis suggests significant but less than equal charge sharing, with more excess charge residing on the O_2 moiety.

The description of the complex anions to this point pertains to the lowest-energy doublet states. Quartet states can also result from the combination of the D_0 state of the glyoxal anion and the neutral $^3\Sigma_g^-$ ground state of O_2. The resulting quartet complex anion can be described as the D_0 state of the glyoxal anion solvated by O_2, with no significant charge transfer and much longer C−O_2 distances. The energy of the quartet complex anion is nearly identical to that of the calculated glyoxal (D_0) + O_2 ($^3\Sigma_g^-$) asymptote, indicating a very weak interaction between the glyoxal anion and neutral O_2.

https://doi.org/10.1021/acs.jpca.1c07163
J. Phys. Chem. A 2021, 125, 9128−9142

Table 3. Bond Distances in Structures Optimized at the CCSD(T) Level for the Anion and Neutral of O_2, *cis*-Glyoxal, and the $[O_2$-*cis*-Glyoxal$]^-$ Complex Anion[a]

molecule	C−C (exp)	C=O	O−O
O_2			1.213 (1.2075)[b]
O_2^-			1.355 (1.348)[c]
trans-glyoxal	1.521 (1.526)[d]	1.211 (1.212)[d]	
cis-glyoxal	1.538 (1.505)[e]	1.208	
[*trans*-glyoxal]$^-$	1.430	1.271	
[*cis*-glyoxal]$^-$	1.442	1.260	
[O_2-*trans*-glyoxal]$^-$	1.491	1.227/1.235[f]	1.309
[O_2-*cis*-glyoxal]$^-$	1.510	1.225	1.318

[a]Bond distances are in units of angstroms. Experimental values are in parentheses. [b]Ref 56. [c]Ref 25. [d]Ref 95. [e]Ref 96. [f]The two CO bonds in [O_2-*trans*-glyoxal]$^-$ are not symmetry-equivalent.

Direct Detachment Transitions. Before considering other excited states of the anion, we discuss the nature of the neutrals that would be accessed via photodetachment of the ground state of the complex anion. The main feature of the neutral bimolecular systems is the flat, effectively repulsive potential. OO-MP2/CCSD(T) calculations predict the O_2 ($^3\Sigma_g^-$)·*trans*-glyoxal van der Waals complex to be bound by 0.02 eV relative to the O_2 ($^3\Sigma_g^-$) + *trans*-glyoxal dissociation limit and the *cis* conformer to be bound by 0.04 eV relative to the *cis* dissociation limit. However, harmonic zero-point corrections show that the shallow OO-MP2 minima cannot support any bound vibrational states. While anharmonic corrections or better methods may change this finding, we conclude that the neutral clusters exhibit essentially repulsive interactions.

The EA of the *cis* conformer of the neutral (1.88 eV) is systematically higher than that of the *trans* conformer (1.71 eV) because, as noted above, the two conformers of the anion are predicted to be very close in energy while calculations predict the *cis* conformer of the neutral to lie 0.2 eV higher in energy than the *trans* conformer, in good agreement with experimental results.[38] Again, these CCSD(T)//OO-MP2 calculated values are summarized in Table 2.

Both the MP2 and CCSD(T)//OO-MP2 calculations predict very broad detachment transitions. As noted above, the CCSD(T)//OO-MP2 calculated ADE value for detachment to the O_2($^3\Sigma_g^-$)·*cis*-glyoxal van der Waals complex, which involves creating a hole in the doubly occupied O_2 π_g-like orbital, is 1.87 eV, while the associated VDE value is 2.94 eV, more than 1 eV above the ADE. This breadth reflects significant differences between the anion and neutral complex structures, associated with the large change in the equilibrium intermolecular distance in addition to a significant difference among the O−O, C−C, and C−O bond lengths in the anion and neutral. Hence, the neutral bimolecular complex is prepared in a intramolecular vibrationally excited state and on the repulsive wall of the neutral intermolecular potential: the partial covalent C−O_2 bond in the anionic complexes (<2.5 Å) is much shorter than the typical intermolecular distance of a van der Waals complex (typically 3.5 Å or greater). The direct detachment signal discernible in the PE spectra of [O_2-methylglyoxal]$^-$ and [O_2-biacetyl]$^-$ is consistent with the predicted breadth of the detachment transitions.

The lowest-energy singlet states of the complexes, which correlate with the O_2 ($^1\Delta_g$) + M (S_0) neutrals, have multireference character and require higher-level calculations. However, on the basis of the experimentally determined term energy of the $^1\Delta_g$ state of O_2 and the calculated energy of the complex anion, we can estimate the ADE value for this transition to be 2.7 eV for the *trans* conformer and 2.9 eV for the *cis* conformer. The VDE is more difficult to approximate, but assuming the same repulsion energy for the singlet neutral state (1.11 eV for the *trans* conformer, 1.02 eV for the *cis* conformer), the VDEs would be >3.7 eV, which exceeds the energy range accessed with the available photon energy.

Excited States of the Complex Anions. Experimentally, the spectra are dominated by the near-threshold signal for all three complexes rather than a direct detachment signal associated with the triplet and singlet neutral states. The near-threshold autodetachment signal points to an excited state of the complex anion. We consider potential excited states.

Figure 1 incorporates the main results from the CCSD(T)//OO-MP2 calculations with experimental energies of the isolated molecules. In addition to the nearly isoenergetic *trans* and *cis* conformers of the [O_2-glyoxal]$^-$ complex, which have a doublet spin state (D_0), a low-lying doublet excited state (D_1) arises from the broken degeneracy of the O_2 π_g orbital due to interactions with glyoxal. The CCSD(T) calculations on [O_2-*cis*-glyoxal]$^-$ predict a $D_1 - D_0$ transition energy of 0.21 eV. Figure 6 shows depictions of the singly and doubly occupied O_2 local orbitals based on CAM-B3LYP calculations on the [O_2-*cis*-glyoxal]$^-$ anion. For comparison with a simple ion−molecule complex, the frontier orbitals in the O_2^-· hexane complex studied previously are also included.[18] The $D_1 - D_0$ transition involves the promotion of an electron from the doubly occupied O_2 π_g orbital, which has a lobe pointing toward and overlapping with the C−C lobe of the π_3 LUMO of glyoxal (singly occupied in the bare glyoxal anion), to the singly occupied π_g, which is oriented parallel to the C−C bond and does not overlap with glyoxal local orbitals. The term energy of the D_1 state is too low to be involved in the autodetachment signal.

A characteristic that often accompanies autodetachment in simple molecular anion PE spectra is a neutral dipole moment sufficiently large to support a dipole bound electron, which is a nonvalence bound state. Because the binding energy of dipole bound electrons is typically on the order of meV, vibrational excitation is usually sufficient to elevate the energy of the dipole bound state (DBS) above the detachment continuum. The excess electron undergoes autodetachment, with e$^-$KE equal to the energy difference between the quasibound level of the anion and the final vibronic level of the neutral.

Table 4 summarizes the computed dipole moments of bare glyoxal, the optimized O_2·glyoxal van der Waals complexes, and the neutral complexes confined to the OO-MP2-optimized structure of the anion. By symmetry, bare *trans*-glyoxal has no dipole moment. The neutral optimized van der Waals complex and the neutral complex confined to the structure of the [O_2-

https://doi.org/10.1021/acs.jpca.1c07163
J. Phys. Chem. A 2021, 125, 9128−9142

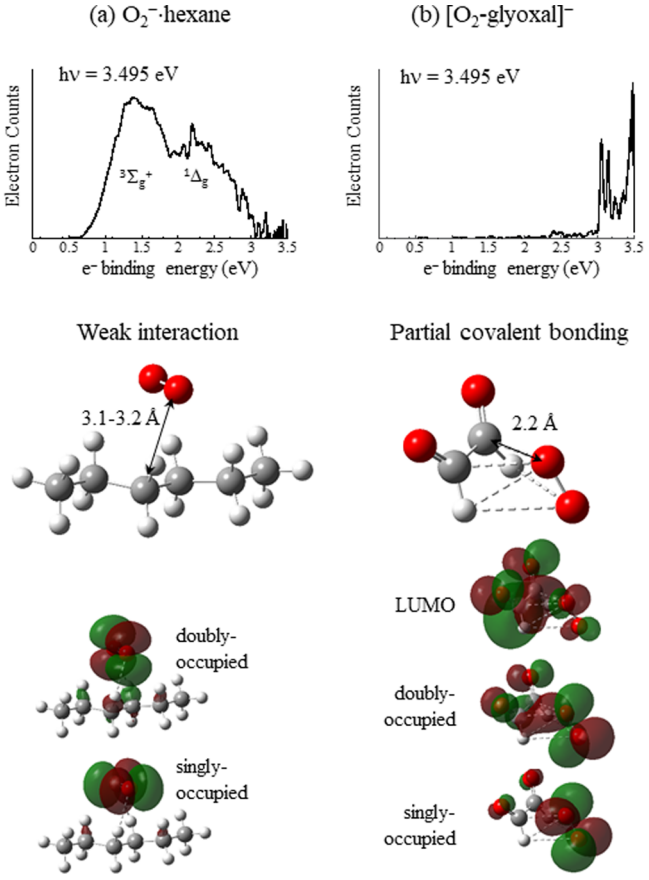

Figure 6. Anion PE spectra, molecular structures, and frontier orbitals of the (a) O_2^-·hexane ion−molecule complex and the (b) [O_2-glyoxal]$^-$ complex anion, highlighting the large difference in O−C internuclear distances between the two species as well as the orbital mixing in the latter, based on CAM-B3LYP calculations on both anions. The O_2^-·hexane spectrum is adapted from ref 18.

Table 4. Dipole Moments of Glyoxal, O_2·Glyoxal van der Waals Complexes, and Neutral Complexes Confined to the Structure of the [O_2-Glyoxal]$^-$ Complex Anion, Calculated at the OO-MP2/def2-TZVPPD Level

molecule or complex	dipole moment (Debye)
trans-glyoxal (C_{2h})	
cis-glyoxal (C_{2v})	3.43
O_2·*trans*-glyoxal	0.26
O_2·*cis*-glyoxal	3.49
O_2·*trans*-glyoxal[a]	1.20
O_2·*cis*-glyoxal[a]	3.79

[a]Confined to the structure of the complex anion.

trans-glyoxal]$^-$ complex anion have nonzero dipole moments but are below the practical minimum dipole moment (2.4−2.5 D)[97,98] necessary to support a DBS. On the other hand, *cis*-glyoxal, the O_2·*cis*-glyoxal van der Waals complex, and the neutral complex confined to the structure of the complex anion have sufficiently large dipole moments, all >3.4 D, to support a DBS by 0.017−0.018 eV or 140−145 cm^{-1} (EOM-CCSD computations). A depiction of the delocalized dipole-bound electron orbital is shown in Figure 7.

We also consider excited valence anion states based on experimental anion asymptotes shown in Figure 1. The T_1 state of glyoxal has a term energy of 2.381 eV,[26] as shown

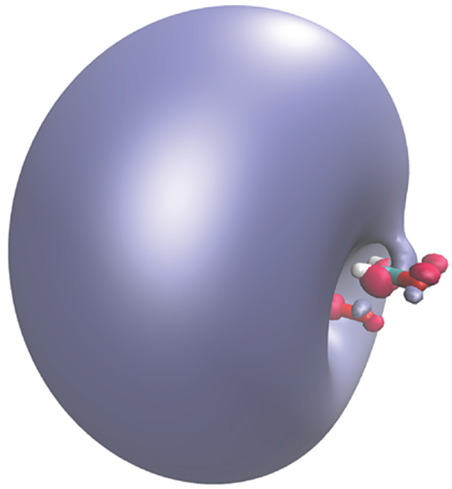

Figure 7. Depiction of the highest occupied molecular orbital of the [O_2-*cis*-glyoxal]$^-$ dipole bound state (0.0026 isosurface). The complex anion structure is confined to the optimized structure of the ground state of the anion. Red represents O, white represents H, and cyan represents C.

schematically in Figure 1 (dashed black lines). A complex anion that correlates to this O_2^- ($^2\Pi_g$) + glyoxal (T_1) limit would therefore lie at least several tenths of an eV below this limit, potentially placing it in the range of the 3.495 eV photon energy. The O_2^- ($^2\Pi_g$) + glyoxal (S_1) excited-state limit is approximately 0.3 eV higher in energy.[99] A transition to either state would involve the promotion of an electron from the nonbonding glyoxal in-plane orbital (n_, the HOMO of the bare glyoxal neutral) to the π_3 orbital, which has overlap with the O_2 π_g orbital. In addition, calculations on the bare glyoxal anion suggest that the D_1 state of the isolated anion, which has appeared as a shape resonance in electron transmission spectra of glyoxal at e$^-$KE ≈ 1.55−2.4 eV,[52,100] is predicted to lie approximately 3.5 eV above the bound D_0 ground state of the isolated glyoxal anion. This temporary anion state, which is accessed via the $\pi_3 \rightarrow \pi_4$ transition in the D_0 state of the isolated glyoxal anion, could potentially form a quasibound complex anion with O_2. In the simplest one-electron framework, it would be accessed from the initial D_0 state of [O_2-glyoxal]$^-$ by the promotion of an electron from the doubly occupied largely O_2 π^* orbital to the π_4 orbital localized on glyoxal.

Excited electronic states of the complex anions embedded in the detachment continuum may be involved in the near-threshold autodetachment signal or, possibly, band **B** in the PE spectrum of [O_2-glyoxal]$^-$. However, other constitutional isomers could potentially be populating the ion beam. We consider several isomers identified computationally.

Additional Possible Anionic Isomers. Peroxyacid structures formed between O_2 and glyoxal or methylglyoxal, with formulas $C_2H_2O_4^-$ and $C_2HCH_3O_4^-$, respectively, are predicted to be 1.5 eV lower in energy than the [O_2−***M***]$^-$ complexes in Figure 5. The analogous bond-insertion adduct for the O_2 + biacetyl anion would require insertion into a C−CH_3 bond, and this structural motif was not pursued; the lowest-energy anion structure was instead found to be the [O_2-biacetyl]$^-$ complex. Other biacetyl adducts with hydrogen transfer were found to be significantly higher in energy. The peroxyacids and peroxides (formed via −H transfer to one of the carbonyl O atoms) are predicted to have EAs of *ca.* 1 eV, which is much lower than any observed detachment transitions, except for the signal that could

https://doi.org/10.1021/acs.jpca.1c07163
J. Phys. Chem. A 2021, 125, 9128−9142

also be attributed to bare O_2^- and glyoxal$^-$ detachment. The relative energies vary slightly with ***M***, as summarized in the Supporting Information.

The fact that the most stable constitutional isomers of $[O_2$-glyoxal$]^-$ and $[O_2$-methylglyoxal$]^-$ are not formed in the source is consistent with our previous studies on ion−molecule complexes. The discharge source used to generate the ions creates free electrons that can attach to molecules with collisional cooling that also facilitates bimolecular complex formation. This process is more prevalent than the bond destruction followed by new bond formation necessary to produce the constitutional isomers that happen to be thermodynamically more stable than the complex anions.

Finally, the class of structures that can be described as O_2 adducts with no further bond rearrangements in the ***M*** partners are predicted to be less stable than their $[O_2{-}\boldsymbol{M}]^-$ counterparts by approximately 0.3−0.5 eV. Calculations predict neutral EA values of approximately 2.5 eV, which is significantly higher than the onset of signal observed in the experimental spectra. Furthermore, OO-MP2 calculations on the covalently bound anionic adduct suggest no barrier to $[O_2{-}\boldsymbol{M}]^-$ formation.

To summarize the computational results in the context of the observed spectra, structures that can be described as constitutional isomers of $[O_2{-}\boldsymbol{M}]^-$, such as the peroxyacids, peroxides, and direct adducts, are not consistent with the direct detachment signal observed definitively in the spectra of $[O_2$-methyglyoxal$]^-$ and $[O_2$-biacetyl$]^-$ and are not consistent with the signal that is unique to the $[O_2$-glyoxal$]^-$ spectrum. A DBS is supported by the O_2-*cis*-glyoxal complex and, by extension, the other O_2-*cis*-***M*** complexes. We consider the most feasible explanation for the appearance of the spectra in the Discussion section.

DISCUSSION

With the experimental spectra and theoretical results, we now attempt to describe the complex anions and provide a more general description of the direct and indirect detachment processes.

Complex Anions. The description of a bimolecular complex anion in which both molecules have positive and comparable EAs has proven to have nuances. In the case of O_2 and glyoxal, the EA of glyoxal exceeds that of O_2 by 0.6 eV, yet most of the charge is carried by O_2. For this particular case, the rationale is that the glyoxal neutral stabilizes O_2^- more than O_2 stabilizes glyoxal (*cis* and *trans* conformers). Previous studies on $O_3^-(O_2)_n$ clusters showed that O_2 molecules stabilized O_3^- by less than 0.1 eV,[57] while polar molecules such as acetone and ethanol were found to stabilize O_2^- by 0.9−1.1 eV.[19] This difference in stabilization (or solvation) energy exceeds the difference in EA of O_2 and glyoxal.

The full picture is more complex, however. The highest-energy doubly occupied orbital can be described as delocalized between the O_2 π^* orbital and what is the SOMO of the isolated glyoxal anion (π_3). Therefore, charge delocalization further stabilizes the complex anion.

Near-Zero e$^-$KE Autodetachment Signal. Both the $[O_2$-methyglyoxal$]^-$ and $[O_2$-biacetyl$]^-$ PE spectra exhibit a feature (band **X**) that can be readily reconciled with the calculated ADEs and VDEs for the complex anions. However, this direct detachment signal is low in intensity relative to the threshold signal in spectra collected with all three photon energies. The threshold signal shared by all three $[O_2{-}\boldsymbol{M}]^-$ PE spectra very likely has a common explanation: it is reasonable to assume that both the *cis*- and *trans*-***M*** conformers of the complex anions populate the ion beam. This assumption is based on the CCSD(T)-calculated energies being within 0.02 eV. Consider Figure 1(b), which shows the energy of the DBS of the $[O_2$-*cis*-glyoxal$]$ complex (gray dots) lying 0.017 eV below the Leonard-Jones potential of the $O_2(^3\Sigma_g^-)$·*cis*-glyoxal van der Waals complex. Any photon energy sufficient to detach an electron will be resonant with a dipole bound state. Over the photon energy range used in this study, all of which lie above the detachment continuum and the O_2 $(^3\Sigma_g^-)$ + ***M*** neutral dissociation limit, the DBS would thus be occupied and would account for the autodetachment features observed near the threshold.

Sanov and co-workers observed threshold autodetachment signal in biacetyl cluster anion PE spectra.[24] They also observed much higher solvation energy than what would be expected in an IMC, which they attributed to the delocalization of charge in the molecular cluster. They attributed the threshold signal to autodetachment from excited states of the complex anions. Here, we suggest that the threshold signal is due to nonvalence bound states.

Unlike more commonly encountered DBSs in which the neutral core is a stable molecule with a large dipole moment, in the case of the $[O_2{-}\boldsymbol{M}]^-$ species, the complex supporting the DBS is unstable with respect to dissociation to isolated O_2 and ***M***. Typically, vibrational autodetachment follows a $\Delta v = -1$ propensity rule, where 1 quantum of relaxation in the neutral core is associated with the ejection of the electron, in a classic example of the breakdown of the Born−Oppenheimer approximation. In the case of these complexes, the relaxation path could easily be a combination of vibrational relaxation of the *cis*-***M*** portion of the complex and the dissociation of the bimolecular complex.

The intensity of the threshold signal indicates that the absorption cross section for accessing the DBS is large compared to direct detachment. A related effect was observed in the PE spectra of ligated gold clusters, for which the direct detachment signal was eliminated when the photon energy was resonant with an excited state of the anion, resulting exclusively in the appearance of thermionic emission.[101] The profile of the threshold signal observed in this study is not consistent with thermionic emission, but both processes are indirect and preceded by an electronic absorption transition.

Spectroscopic Features Unique to the $[O_2$-Glyoxal$]^-$ PE Spectrum. Band **A** in the PE spectrum of $[O_2$-glyoxal$]^-$ collected with 2.883 eV and band **B** in the spectrum obtained with 3.495 eV are more difficult to explain than the signal near the threshold. Band **X** is at an energy that is in reasonable agreement with the calculated $O_2(^3\Sigma_g^-)$·glyoxal $(S_0) \leftarrow [O_2$-glyoxal$]^-$ detachment transition, and the broad continuum signal in the 1.9−2.3 eV e$^-$BE range can be assigned to this transition. Band **A**, a narrower feature which changes in relative intensity over the 2.864 to 2.895 eV energy range, cannot be reconciled with a direct detachment transition to a van der Waals complex. The variation in the signal with small changes in photon energy suggests tuning through the vibrational levels of a temporary anion state. Any of the several close-lying excited states described above, such as the glyoxal anion coupled with the neutral $^1\Sigma_g^+$ state of O_2, are potentially involved in the appearance of this signal.

Band **B** in the 3.495 eV spectrum of $[O_2$-glyoxal$]^-$, with the cleanly resolved 800 cm^{-1} progression, is very different in appearance than band **A** and is evocative of a diatomic or high-symmetry molecule. The higher-lying excited states of O_2

https://doi.org/10.1021/acs.jpca.1c07163
J. Phys. Chem. A 2021, 125, 9128−9142

accessed via $\pi_u \rightarrow \pi_g$ transitions have frequencies of approximately 800 cm^{-1},[56] though any detachment transitions associated with the O_2^--local π_u orbital would be *ca.* 4 eV, which is higher than the photon energy used in this study. The C−C stretch in *cis*-glyoxal is 826 cm^{-1}, and the C═O symmetric stretch is 1746 cm^{-1}.[79] Both could be active in a direct or indirect detachment transition, given the change in charge localized in the π_3 orbital upon electron ejection from the complex. As noted earlier, *trans*-glyoxal has an 801 cm^{-1} mode,[77,78] but the complex does not support a DBS.

The profile of band **B** is similar to transitions to the lowest triplet states of methylglyoxal and biacetyl observed in the PE spectra of their respective bare anions. However, the e^-BE at which this band is observed, 3.05 eV, is lower than the transition energy anticipated for the bare glyoxal anion. (T_0 = 2.381 eV relative to the S_0 state of glyoxal and therefore 3.481 eV relative to the bare glyoxal anion.)

We consider other electronic states of the complex anion that might be uniquely contributing to the spectrum of $[O_2$-glyoxal$]^-$.

First, we consider excitation to temporary anion states followed by electron ejection. Given that O_2 carries more charge than glyoxal in the complex anion, a glyoxal-local transition would be similar in energy to bare glyoxal excitations. The glyoxal $S_0 \rightarrow S_1$ transition energy is 2.72 eV,[99] just above the $S_0 \rightarrow T_1$ transition (2.38 eV). These transitions are the spin-allowed and spin-forbidden n _ → π_3 transitions. The $[O_2{-}S_1]^-$ or $[O_2{-}T_1]^-$ temporary anion states may be long-lived; the lifetimes of the isolated glyoxal excited states are 2.4 μs and 3.29 ms for the S_1 and T_1 states, respectively,[102] which are long compared to lifetimes of typical vibrationally excited nonvalence bound states. However, the autodetachment process would be complex, involving photorelaxation coupled with the ejection of the π_g electron from the $O_2^{-2}\Pi_u$ partner (i.e., an electronic autodetachment process).

Given the e^-KEs of the observed signal, the final neutral state would be the O_2 ($^1\Delta_g$)·glyoxal (S_0) complex. The 800 cm^{-1} spacing is consistent with the experimental C−C stretch of *cis*-glyoxal[79] and the calculated butterfly bending mode (with the C−C bond being the butterfly's body, Supporting Information), which is relevant because the π_3 orbital is C−C bonding and glyoxal is slightly nonplanar in the complex anion.

The observed progression in band **B** is difficult to reconcile with this scenario since it would involve large changes in vibrational quanta from the quasibound complex anion and the final neutral levels. However, large changes in the vibrational quantum level have been seen in vibrational autodetachment from the quasibound vibrational levels of O_2^- ($v > 3$), with Δv = −7, −6, −5, −4 having been observed.[57] In cases where the autodetaching and final neutral states have minimum energies that differ by far more than a vibrational spacing or have different structures (unlike the case of a DBS of a molecule in which the dipole bound anion is structurally identical to the neutral molecule), the Δv = −1 propensity rule is not always energetically possible.

A similarly complex autodetachment process would be excitation to the complex anion that correlates to the glyoxal$^-$ (D_1) + O_2 ($^3\Sigma_g^-$) asymptote, which is the sole asymptote that does not have an accurate, experimentally determined energy shown in Figure 1(a,b).[52] However, this anion would be modestly stabilized relative to the glyoxal S_0 neutral due to the presence of O_2. Again, given the e^-KE of the observed signal, the final neutral state would be the O_2 ($^1\Delta_g$)·glyoxal (S_0) complex, requiring electron ejection with a forbidden transition in the nominally neutral O_2 partner.

This discussion invokes numerous electronic states of the complex arising from the combination of close-lying states of the constituent molecules as well as charge delocalization in the complex anion. Given the challenges of theoretically characterizing this manifold of states, any explanation for this vibrational progression with isotropic PAD is speculative. However, the strong coupling between O_2 and glyoxal in the complex anion relative to the methylated analogs and the several electronic excited states that are accessible only with the highest photon energy used in this study, combined with the significant differences in the appearances of the spectra measured with different photon energies, suggests that an excited state of the complex anion undergoes delayed electron ejection. The distribution of final vibrational states of the glyoxal appears to be encoded in the e^-KEs.

Nonvalence bound anion states (such as a DBS), in which an electron is bound by long-range interactions between a neutral core and the electron, and temporary anion states, such as the D_1 state of the glyoxal anion that lies over 1.5 eV above the neutral, play an important role in the electron attachment processes that occur in fields that range from DNA damage[103−106] to astrochemistry[105,106] and may govern electron-driven chemistry in some systems. Excitation to these states from valence-bound anionic precursors such as those presented here provides a back-door view of these processes and, it is hoped, will provide essential data for subsequent theoretical studies on these systems.

CONCLUSIONS

PE spectra of the $[O_2{-}\boldsymbol{M}]^-$ (***M*** = glyoxal, methylglyoxal, or biacetyl) complex anions were presented and interpreted with supporting calculations on both the anionic and neutral complexes. Previously reported studies on a series of O_2^-·VOC IMCs confirmed that the excess charge was definitively carried by O_2. The resulting PE spectra reflected the electronic structure of O_2 but shifted to higher binding energy due to the extra stabilization of O_2^- by the VOC. In contrast, these $[O_2{-}\boldsymbol{M}]^-$ complex anions defy being characterized as IMCs. The photoelectron spectra of the $[O_2{-}\boldsymbol{M}]^-$ complex anions show very low-intensity direct detachment signal. Over a range of photon energies, the spectra are all dominated by a near-threshold autodetachment signal. The low-intensity direct-detachment signal is a broad continuum for all three species, suggesting a very significant difference between the stable anion and neutral structures. The spectrum of $[O_2$-glyoxal$]^-$ obtained with 2.330 eV photon energy showed evidence of photodissociation to O_2 + glyoxal$^-$, followed by detachment of free glyoxal, and the spectrum of $[O_2$·biacetyl$]^-$ similarly showed evidence of photodissociation to O_2^- + biacetyl.

Results of calculations on the neutral O_2·glyoxal complexes confined to the structure of the complex anions suggest that the very large dipole moment of *cis*-glyoxal can support a dipole bound state over a range of O_2···glyoxal intermolecular distances. Moreover, while the O_2·*cis*-glyoxal neutral lies 0.20 eV higher in energy than the O_2·*trans*-glyoxal conformer, the two conformers of the anion are nearly isoenergetic. We therefore attribute the threshold autodetachment to a dipole-bound anion that is resonant with every photon energy used in this study because of the Franck−Condon overlap between the initial anion state with a steeply repulsive (continuum) part of the $O_2{-}\boldsymbol{M}$ intermolecular potential. Finally, calculations suggest partial

https://doi.org/10.1021/acs.jpca.1c07163
J. Phys. Chem. A 2021, 125, 9128−9142

covalent bond formation between O_2 and ***M*** in the complex anions, with more charge carried by O_2 and the remainder localized in the π_3 orbital of ***M***. Partial bonding and the potential capture of free electrons while two molecules with competing EA undergo a collision are new insights gleaned from this study.

The $[O_2$-glyoxal$]^-$ spectra obtained using 2.883 and 3.495 eV photon energies also exhibited features at ∼0.5 eV e^-KE that cannot be assigned to direct detachment transitions from the complex anion or other constitutional isomers. There are numerous excited electronic states of the complex anion, several of which were considered to be sources of this signal. Further efforts to characterize the nature of the state involved in this unique feature are ongoing.

■ ASSOCIATED CONTENT

Supporting Information

The Supporting Information is available free of charge at https://pubs.acs.org/doi/10.1021/acs.jpca.1c07163.

Raw and reconstructed images for the PE spectra shown in Figures 2−4; comparison of the O_2^-·acetone IMC PE spectrum with the spectra of the complex anions presented in this report; comparison of the spectral e^- KE distribution with a thermionic emission distribution function and a simple exponential decay function; spectra collected over 50 cm^{-1} steps of the $[O_2$-methylglyoxal$]^-$ and $[O_2$-biacetyl$]^-$ complex anions in the 2.864−2.895 eV range; 3.495 eV spectra of the complexes resolved into parallel and perpendicular electron distributions; comprehensive relative energies of the complexes and constitutional isomers calculated at the MP2 level; and vibrational frequencies and normal coordinates calculated for the triplet and singlet states of the *cis* and *trans* conformers of the O_2·glyoxal neutral complexes calculated to be bound using the CAM-B3LYP and MP2 methods (PDF)

■ AUTHOR INFORMATION

Corresponding Authors

Thomas Sommerfeld − *Department of Chemistry and Physics, Southeast Louisiana University, Hammond, Louisiana 70402, United States;* orcid.org/0000-0001-8105-5414; Email: Thomas.Sommerfeld@southeastern.edu

Caroline Chick Jarrold − *Department of Chemistry, Indiana University, Bloomington, Indiana 47405, United States;* orcid.org/0000-0001-9725-4581; Email: cjarrold@indiana.edu

Authors

Marissa A. Dobulis − *Department of Chemistry, Indiana University, Bloomington, Indiana 47405, United States*

Conor J. McGee − *Department of Chemistry, Indiana University, Bloomington, Indiana 47405, United States*

Complete contact information is available at: https://pubs.acs.org/10.1021/acs.jpca.1c07163

Notes

The authors declare no competing financial interest.

■ ACKNOWLEDGMENTS

This material is based upon work supported by the National Science Foundation under grant nos. 2053889 and 1664965 (C.C.J.) and grant no. 1856775 (T.S.).

■ REFERENCES

(1) Markus, C. R.; Asvany, O.; Salomon, T.; Schmid, P. C.; Brünken, S.; Lipparini, F.; Gauss, J.; Schlemmer, S. Vibrational Excitation Hindering an Ion−Molecule Reaction: The c-C3H2+-H2 Collision Complex. *Phys. Rev. Lett.* **2020**, *124*, 223401.

(2) Squires, R. R.; Bierbaum, V. M.; Grabowski, J. J.; DePuy, C. H. Multiple Proton Transfers within Long-Lived Ion Molecule Complexes. *J. Am. Chem. Soc.* **1983**, *105*, 5185−5192.

(3) Ingemann, S.; Nibbering, N. M. M.; Sullivan, S. A.; DePuy, C. H. Nucleophilic Aromatic Substitution in the Gas Phase: The Importance of Fluoride Ion−Molecule Complexes Formed in Gas-Phase Reactions Between Nucleophiles and Some Alkyl Pentafluorophenyl Ethers. *J. Am. Chem. Soc.* **1982**, *104*, 6520−6527.

(4) Willey, K. F.; Cheng, P. Y.; Bishop, M. B.; Duncan, M. A. Charge-Transfer Photochemistry in Ion−Molecule Complexes of Silver. *J. Am. Chem. Soc.* **1991**, *113*, 4721−4728.

(5) Yang, X.; Hu, Y.; Yang, S. Photoinduced Reactions in the Ion−Molecule Complexes Mg+-XCH3 (X = F, Cl). *J. Phys. Chem. A* **2000**, *104*, 8496−8504.

(6) Morton, T. H. Ion Molecule Complexes in Unimolecular Fragmentation of Gaseous Cations. Alkyl Phenyl Ether Molecular Ions. *J. Am. Chem. Soc.* **1980**, *102*, 1596−1602.

(7) Sheng, H.; Tang, W.; Yerabolu, R.; Max, J.; Kotha, R. R.; Riedeman, J. S.; Nash, J. J.; Zhang, M.; Kenttämaa, H. I. Identification of N-Oxide and Sulfoxide Functionalities in Protonated Drug Metabolites by Using Ion-Molecular Reactions Followed by Collisionally Activated Dissociation in a Linear Quadrupole Ion Trap Mass Spectrometer. *J. Org. Chem.* **2016**, *81*, 575−586.

(8) Zhu, H.; Ma, X.; Kong, J. Y.; Zhang, M.; Kenttämaa, H. I. Identification of Carboxylate, Phosphate, and Phenoxide Functionalities in Deprotonated Molecules Related to Drug Metabolites via Ion−Molecule Reactions with Water and Diethylhydroxyborane. *J. Am. Soc. Mass Spectrom.* **2017**, *28*, 2189−2200.

(9) Wu, C.-X.; Hu, J.; He, M.-M.; Zhi, Y.; Tian, S. X. Ion Momentum Imaging Study of the Ion−Molecule Reaction Ar+ + O2 → O2+ + Ar. *Phys. Chem. Chem. Phys.* **2020**, *22*, 4640−4646.

(10) Thøgersen, J.; Réhault, J.; Odelius, M.; Ogden, T.; Jena, N. K.; Jensen, S. J. K.; Keiding, S. R.; Helbing, J. Hydration Dynamics of Aqueous Nitrate. *J. Phys. Chem. B* **2013**, *117*, 3376−3388.

(11) Yuan, R.; Yan, C.; Fayer, M. Ion−Molecule Complex Dissociation and Formation Dynamics in LiCl Aqueous Solutions from 2D IR Spectroscopy. *J. Phys. Chem. B* **2018**, *122*, 10582−10592.

(12) Waterland, M. R.; Stockwell, D.; Kelley, A. M. Symmetry Breaking Effects of $NO3^-$: Raman Spectra of Nitrate Salts and Ab Initio Resonance Raman Spectra of Nitrate-Water Complexes. *J. Chem. Phys.* **2001**, *114*, 6249.

(13) Vuitton, V.; Yelle, R. V.; Klippenstein, S. J.; Hörst, S. M.; Lavvas, P. Simulating the Density of Organic Species in the Atmosphere of Titan With a Coupled Ion-Neutral Photochemical Model. *Icarus* **2019**, *324*, 120−197.

(14) Larsson, M.; Geppert, W. D.; Nyman, G. Ion Chemistry in Space. *Rep. Prog. Phys.* **2012**, *75*, 066901.

(15) Viggiano, A. A. Reexamination of Ionospheric Chemistry: High Temperature Kinetics, Internal Energy Dependences, Usual Isomers, and Corrections. *Phys. Chem. Chem. Phys.* **2006**, *8*, 2557−2571.

(16) Anicich, V. G.; McEwan, M. J. Ion−Molecule Chemistry in Titan's Ionosphere. *Planet. Space Sci.* **1997**, *45*, 897−921.

(17) Richards, D. S.; Trobaugh, K. L.; Hajak-Herrera, J.; Price, C. L.; Sheldon, C. S.; Davies, J. F.; Davis, R. D. Ion−Molecule Interactions Enable Unexpected Phase Transitions in Organic-Inorganic Aerosol. *Sci. Adv.* **2020**, *6*, No. eabb5643.

(18) Patros, K. M.; Mann, J. E.; Jarrold, C. C. Photoelectron Imaging Spectra of O_2^-·VOC and O_4^-·VOC Complexes. *J. Phys. Chem. A* **2016**, *120*, 7828−7838.

(19) Patros, K. M.; Mann, J. E.; Jarrold, C. C. O_2^-·[Polar VOC] Complexes: H-Bonding versus Charge-Dipole Interactions, and the Noninnocence of Formaldehyde. *J. Phys. Chem. A* **2017**, *121*, 5459−5467.

(20) Dobulis, M. A.; Thompson, M. C.; Sommerfeld, T.; Jarrold, C. C. Temporary Anion States of Fluorine Substituted Benzenes Probed by Charge Transfer in O_2^-·C6H6-xFx (x = 0−5) Ion−Molecule Complexes. *J. Chem. Phys.* **2020**, *152*, 204309.
(21) Driver, N.; Jena, P. Electron Affinity of Modified Benzene. *Int. J. Quantum Chem.* **2018**, *118*, No. e25504.
(22) Xue, T.; Dixon, A. R.; Sanov, A. Anion Photoelectron Imaging Spectroscopy of Glyoxal. *Chem. Phys. Lett.* **2016**, *660*, 205−208.
(23) Dauletyarov, Y.; Dixon, A. R.; Wallace, A. A.; Sanov, A. Electron Affinity and Excited States of Methylglyoxal. *J. Chem. Phys.* **2017**, *147*, 013934.
(24) Dauletyarov, Y.; Wallace, A. A.; Blackstone, C. C.; Sanov, A. Photoelectron Spectroscopy of Biacetyl and Its Cluster Anions. *J. Phys. Chem. A* **2019**, *123*, 4158−4167.
(25) Ervin, K. M.; Anusiewicz, I.; Skurski, P.; Simons, J.; Lineberger, W. C. The Only Stable State of O_2^- is the $X^2\Pi_g$ Ground State and It (Still!) Has an Adiabatic Electron Detachment Energy of 0.45 eV. *J. Phys. Chem. A* **2003**, *107*, 8521−8529.
(26) Spangler, L. H.; Pratt, D. W. Laser-Induced Phosphorescence Spectroscopy in Supersonic Jets - The Lowest Triplet-States of Glyoxal, Methylglyoxal, and Biacetyl. *J. Chem. Phys.* **1986**, *84*, 4789−4796.
(27) Wittrock, F.; Richter, A.; Burrows, J. P.; Vrekoussis, M.; Henze, D. K. Simultaneous Global Observations of Glyoxal and Formaldehyde from Space. *Geophys. Res. Lett.* **2006**, *33*, L16804.
(28) Volkamer, R.; Platt, U.; Wirtz, K. Primary and Secondary Glyoxal Formation from Aromatics: Experimental Evidence for the Bicylcoalkyl-Radical Pathway from Benzene, Toluene, and p-Xylene. *J. Phys. Chem. A* **2001**, *105*, 7865−7874.
(29) Carlton, A. G.; Turpin, B. J.; Altieri, K. E.; Seitzinger, S.; Reff, A.; Lim, H.-J.; Ervens, B. Atmospheric Oxalic Acid and SOA Production from Glyoxal: Results of Aqueous Photooxidation Experiments. *Atmos. Environ.* **2007**, *41*, 7588−7602.
(30) Waxman, E. M.; Dzepina, K.; Ervens, B.; Lee-Taylor, J.; Aumont, B.; Jimenez, J. L.; Madronich, S.; Volkamer, R. Secondary Organic Aerosol Formation from Semi- and Intermediate-Volatility Organic Compounds and Glyoxal: Relevance of O/C as a Tracer for Aqueous Multiphase Chemistry. *Geophys. Res. Lett.* **2013**, *40*, 978−982.
(31) Lombardi, M.; Jost, R.; Michel, C.; Tramer, A. Study of Singlet-Triplet Coupling in Glyoxal by Level Anticrossing Spectroscopy. II. Theory of the Positions of Double Resonances Near a Singlet-Triplet Anticrossing. Application to the Precise Measurement of Singlet-Triplet Coupling and of Fine and Hyperfine Structure Parameters of the Triplet of Glyoxal. *Chem. Phys.* **1981**, *57*, 341−353.
(32) Dupre, P.; Jost, R.; Lombardi, M. Study of Singlet-Triplet Coupling in Glyoxal by Level Anticrossing Spectroscopy. V. Nature of the Singlet-Triplet Interaction. *Chem. Phys.* **1984**, *91*, 355−372.
(33) Michel, C.; Tramer, A. Selected Rotational Level Lifetimes and Singlet-Triplet Coupling in the S_1 State of Glyoxal. *Chem. Phys.* **1979**, *42*, 315−323.
(34) Anderson, L. G.; Parmenter, C. S.; Poland, H. M. Collision Induced Intersystem Crossing. The Photophysics of Glyoxal Vapor Excited at 4358 Å. *Chem. Phys.* **1973**, *1*, 401−417.
(35) Loge, G. W.; Parmenter, C. S. Collision-Free Dissociation after Excitation of Single Rotational Levels in S_1Glyoxal. *J. Phys. Chem.* **1981**, *85*, 1653−1662.
(36) Yardley, J. T. Collisional Quenching and Photochemistry of trans-Glyoxal (3Au) Molecules. *J. Chem. Phys.* **1972**, *56*, 6192.
(37) Diem, M.; MacDonald, B. G.; Lee, E. K. C. Photolysis and Laser-Excited Fluorescence and Phosphorescence Emission of trans-Glyoxal in an Argon Matrix at 13 K. *J. Phys. Chem.* **1981**, *85*, 2227−2232.
(38) Butz, K. W.; Krajnovich, D. J.; Parmenter, C. S. An Experimental Potential Energy Surface for Internal Rotation in Glyoxal. *J. Chem. Phys.* **1990**, *93*, 1557.
(39) Butz, K. W.; Johnson, J. R.; Krajnovich, D. J.; Parmenter, C. S. Cis-Glyoxal in Effusive and Supersonic Beams. Spectroscopy, Selective Pumping, and Cis-Trans Interconversion. *J. Chem. Phys.* **1987**, *86*, 5923.
(40) Smith, D. F.; McIver, C. D.; Kleindienst, T. E. Primary Product Distribution from the Reaction of Hydroxyl Radicals with Toluene at ppb NOx Mixing Ratios. *J. Atmos. Chem.* **1998**, *30*, 209−228.
(41) Bandow, H.; Washida, N. Ring-Cleavage Reactions of Aromatic Hydrocarbons Studied by FT-IR Spectroscopy. III. Photooxidation of 1,2,3-, 1,2,4-, and 1,3,5-Trimethylbenzenes in the NOx-Air System. *Bull. Chem. Soc. Jpn.* **1985**, *58*, 2549−2555.
(42) Paulson, S. E.; Seinfeld, J. H. Development and Evaluation of a Photooxidation Mechanism for Isoprene. *J. Geophys. Res.* **1992**, *97*, 20703−20715.
(43) De Haan, D. O.; Corrigan, A. L.; Tolbert, M. A.; Jimenez, J. L.; Wood, S. E.; Turley, J. J. Secondary Organic Aerosol Formation by Self-Reaction of Methylglyoxal and Glyoxal in Evaporating Droplets. *Environ. Sci. Technol.* **2009**, *43*, 8184−8190.
(44) Schwier, A. N.; Sareen, N.; Mitroo, D.; Shapiro, E. L.; McNeill, V. F. Glyoxal-Methylglyoxal Cross-Reactions in Secondary Organic Aerosol Formation. *Environ. Sci. Technol.* **2010**, *44*, 6174−6182.
(45) Atkinson, R.; Aschmann, S. M. Products of the Gas-Phase Reactions of Aromatic Hydrocarbons: Effects of NO2 Concentration. *Int. J. Chem. Kinet.* **1994**, *26*, 929−944.
(46) Atkinson, R. Atmospheric Chemistry of VOCs and NOx. *Atmos. Environ.* **2000**, *34*, 2063−2101.
(47) Faust, B. C.; Powell, K.; Rao, C. J.; Anastasio, C. Aqueous-Phase Photolysis of Biacetyl (an α-Dicarbonyl Compound): A Sink for Biacetyl, and a Source of Acetic Acid, Peroxyacetic Acid, Hydrogen Peroxide, and the Highly Oxidizing Acetylperoxyl Radical in Aqueous Aerosols, Fogs, and Clouds. *Atmos. Environ.* **1997**, *31*, 497−510.
(48) Chen, Y.; Wang, W.; Zhu, L. Wavelength-Dependent Photolysis of Methylglyoxal in the 290−440 nm Region. *J. Phys. Chem. A* **2000**, *104*, 11126−11131.
(49) Kaya, K.; Harshbarger, W. R.; Robin, M. B. Triplet States of Biacetyl and Energy Transfer as Revealed by Opto-Acoustic Spectroscopy. *J. Chem. Phys.* **1974**, *60*, 4231.
(50) Chaiken, J.; Gurnick, M.; McDonald, J. D. Average Singlet-Triplet Coupling Properties of Biacetyl and Methylglyoxal Using Quantum Beat Spectroscopy. *J. Chem. Phys.* **1981**, *74*, 106.
(51) Verhaart, G. J.; Brongersma, H. H. Triplet $\pi\rightarrow\pi^*$ and $\pi\rightarrow\pi^*$ Transitions in Glyoxal and Biacetyl by Low-Energy Electron-Impact Spectroscopy. *Chem. Phys. Lett.* **1980**, *72*, 176−180.
(52) Senent, M. L.; Moule, D. C.; Smeyers, Y. G.; Torolabbe, A.; Peqalver, F. J. A Theoretical Spectroscopic Study of the $\tilde{A}\ ^1A_u$ (S_1) ←X $^1A_g(S_0)$, n→π^* Transition in Biacetyl, (CH3CO)2. *J. Mol. Spectrosc.* **1994**, *164*, 66−78.
(53) Horowitz, A.; Meller, R.; Moortgat, G. K. The UV-Vis Absorption Cross Sections of α-Dicarbonyl Compounds: Pyruvic Acid, Biacetyl, and Glyoxal. *J. Photochem. Photobiol., A* **2001**, *146*, 19−27.
(54) Opila, R. L.; Coveleski, R. A.; Yardley, J. T. Spectroscopic Confirmation of Reversible Electronic Energy Transfer in Methylglyoxal. *J. Chem. Phys.* **1975**, *63*, 593.
(55) Huber, K. P.; Herzberg, G. Constants of Diatomic Molecules. *Molecular Spectra and Molecular Structure*; Springer: Boston, 1979; pp 494−496. .
(56) Mann, J. E.; Troyer, M. E.; Jarrold, C. C. Photoelectron Imaging and Photodissociation of Ozonide in $O_3^-\cdot(O_2)_n$(n = 1−4) Clusters. *J. Chem. Phys.* **2015**, *142*, 124305.
(57) Duncan, M. A. Infrared Laser Spectroscopy of Mass-Selected Carbocations. *J. Phys. Chem. A* **2012**, *116*, 11477−11491.
(58) Posey, L. A.; Deluca, M. J.; Johnson, M. A. Demonstration of a Pulsed Photoelectron Spectrometer on Mass-Selected Negative Ions: Oπ, $O_2\pi$, and $O_4\pi$. *Chem. Phys. Lett.* **1986**, *131*, 170−174.
(59) Bakker, J. M. B. A Beam-Modulated Time-of-Flight Mass Spectrometer. I. Theoretical Considerations. *J. Phys. E: Sci. Instrum.* **1973**, *6*, 785−789.
(60) Bakker, J. M. B. A Beam-Modulated Time-of-Flight Mass Spectrometer. II. Experimental Work. *J. Phys. E: Sci. Instrum.* **1974**, *7*, 364−368.
(61) Eppink, A. T. J. B.; Parker, D. H. Velocity Map Imaging of Ions and Electrons Using Electrostatic Lenses: Application in Photoelectron

https://doi.org/10.1021/acs.jpca.1c07163
J. Phys. Chem. A 2021, 125, 9128−9142

and Photofragment Ion Imaging of Molecular Oxygen. *Rev. Sci. Instrum.* **1997**, *68*, 3477−3484.
(62) Dribinski, V.; Ossadtchi, A.; Mandelshtam, V. A.; Reisler, H. Reconstruction of Abel-Transformable Images: The Gaussian Basis-Set Expansion Abel Transform Method. *Rev. Sci. Instrum.* **2002**, *73*, 2634−2642.
(63) Cooper, J.; Zare, R. N. Angular Distributions of Photoelectrons. *J. Chem. Phys.* **1968**, *48*, 942−943.
(64) Sanov, A. Laboratory-Frame Photoelectron Angular Distributions in Anion Photodetachment: Insight into Electronic Structure and Intermolecular Interactions. *Annu. Rev. Phys. Chem.* **2014**, *65*, 341−363.
(65) Garcia, G. A.; Nahon, I.; Powis, I. Two-Dimensional Charged Particle Image Inversion Using a Polar Basis Function Expansion. *Rev. Sci. Instrum.* **2004**, *75*, 4989.
(66) Frisch, M. J.; Trucks, G. W.; Schlegel, H. B.; Scuseria, G. E.; Robb, M. A.; Cheeseman, J. R.; Scalmani, G.; Barone, V.; Petersson, G. A.; Nakatsuji, H.; Li, X.; Caricato, M.; Marenich, A. V.; Bloino, J.; Janesko, B. G.; Gomperts, R.; Mennucci, B.; Hratchian, H. P.; Ortiz, J. V.; Izmaylov, A. F.; Sonnenberg, J. L.; Williams-Young, D.; Ding, F.; Lipparini, F.; Egidi, F.; Goings, J.; Peng, B.; Petrone, A.; Henderson, T.; Ranasinghe, D.; Zakrzewski, V. G.; Gao, J.; Rega, N.; Zheng, G.; Liang, W.; Hada, M.; Ehara, M.; Toyota, K.; Fukuda, R.; Hasegawa, J.; Ishida, M.; Nakajima, T.; Honda, Y.; Kitao, O.; Nakai, H.; Vreven, T.; Throssell, K.; Montgomery, J. A., Jr.; Peralta, J. E.; Ogliaro, F.; Bearpark, M. J.; Heyd, J. J.; Brothers, E. N.; Kudin, K. N.; Staroverov, V. N.; Keith, T. A.; Kobayashi, R.; Normand, J.; Raghavachari, K.; Rendell, A. P.; Burant, J. C.; Iyengar, S. S.; Tomasi, J.; Cossi, M.; Millam, J. M.; Klene, M.; Adamo, C.; Cammi, R.; Ochterski, J. W.; Martin, R. L.; Morokuma, K.; Farkas, O.; Foresman, J. B.; Fox, D. J. et al.; *Gaussian 16*, Rev. C.01; Gaussian, Inc.: Wallingford, CT, 2016.
(67) Bozkaya, U. Orbital-Optimized Second-Order Perturbation Theory with Density-Fitting and Cholesky Decomposition Approximations: An Efficient Implementation. *J. Chem. Theory Comput.* **2014**, *10*, 2371−2378.
(68) Weigend, F.; Ahlrichs, R. Balanced Basis Sets of Split Valence, Triple Zeta Valence and Quadrupole Zeta Valence Quality for H to Rn: Design and Assessment of Accuracy. *Phys. Chem. Chem. Phys.* **2005**, *7*, 3297−3305.
(69) Dunning, T. H. Gaussian Basis Sets for use in Correlated Molecular Calculations. I. The Atoms Boron through Neon and Hydrogen. *J. Chem. Phys.* **1989**, *90*, 1007−1023.
(70) Papajak, W.; Zheng, J.; Xu, X.; Leverentz, H. R.; Truhlar, D. G. Perspectives on Basis Sets Beautiful: Seasonal Plantings of Diffuse Basis Functions. *J. Chem. Theory Comput.* **2011**, *7*, 3027−3034.
(71) Chao, J.S.-Y.; Falcetta, M. F.; Jordan, J. D. Application of the Stabilization Method to the N2- (122g) and Mg- (12P) Temporary Anion States. *J. Chem. Phys.* **1990**, *93*, 1125−1135.
(72) Landau, A.; Haritan, I.; Kapralova-Zd'anska, P. R.; Moiseyev, N. Atomic and Molecular Complex Resonances from Real Eigenvalues Using Standard (Hermitian) Electronic Structure Calculations. *J. Phys. Chem. A* **2016**, *120*, 3098−3108.
(73) Neese, F.; Wennmohs, F.; Becker, U.; Riplinger, C. The ORCA Quantum Chemistry Program Package. *J. Chem. Phys.* **2020**, *152*, 224108.
(74) Matthews, D. A.; Cheng, L.; Harding, M. E.; Lipparini, F.; Stopkowicz, S.; Jagau, T.-C.; Szalay, P. G.; Gauss, J.; Stanton, J. F. Coupled-Cluster Techniques for Computational Chemistry: The CFOUR Program Package. *J. Chem. Phys.* **2020**, *152*, 214108.
(75) Profeta, L. T. M.; Sams, R. L.; Johnson, T. J.; Williams, S. D. Quantitative Infrared Intensity Studies of Vapor-Phase Glyoxal, Methylglyoxal, and 2,3-Butanedione (Diacetyl) with Vibrational Assignments. *J. Phys. Chem. A* **2011**, *115*, 9886−9900.
(76) Dong, R. Y.; Nanes, R.; Ramsay, D. A. Rotational Analyses of the Bands of the A^1B^1 -X^1A^1 System of cis-Glyoxal. *Can. J. Chem.* **1993**, *71*, 1595−1597.
(77) Buonaugurio, A.; Graham, J.; Buytendyk, A.; Bowen, K. H.; Ryder, M. R.; Keolopioe, Z. G.; Haranczyk, M.; Gutowski, M. Remarkable Electrophilicity of the Oxalic Acid Monomer: An Anion Photoelectron Spectroscopy and Theoretical Study. *J. Chem. Phys.* **2014**, *140*, 221103.
(78) Mabbs, R.; Mbaiwa, F.; Wie, J.; Van Duzor, M.; Gibson, S. T.; Cavanagh, S. J.; Lewis, B. R. Observation of Vibration-Dependent Electron Anisotropy in $O2^{-\cdot}$Photodetachment. *Phys. Rev. A: At., Mol., Opt. Phys.* **2010**, *82*, No. 011401.
(79) Dao, D. B.; Mabbs, R. The Effect of the Dipole Bound State of AgF- Vibrationally Resolved Photodetachment Cross Sections and Photoelectron Angular Distributions. *J. Chem. Phys.* **2014**, *141*, 154304.
(80) Jagau, T. C.; Dao, D. B.; Holtgrewe, N. S.; Krylov, A. I.; Mabbs, R. Same but Different: Dipole-Stabilized Shape Resonances in $CuF^{-\cdot}$ and AgF^-. *J. Phys. Chem. Lett.* **2015**, *6*, 2786−2793.
(81) Zhu, G.-Z.; Liu, Y.; Wang, L.-S. Observation of Excited Quadrupole-Bound States in Cold Anions. *Phys. Rev. Lett.* **2017**, *119*, 023002.
(82) Huang, D.-L.; Zhu, G.-Z.; Wang, L.-S. Communication: Observation of Dipole-Bound States and High-Resolution Photoelectron Imaging of Cold Acetate Anions. *J. Chem. Phys.* **2015**, *142*, 091103.
(83) Liu, H.-T.; Ning, C.-G.; Huang, D.-L.; Dau, P. D.; Wang, L.-S. Observation of Mode-Specific Vibrational Autodetachment from Dipole-Bound States of Cold Anions. *Angew. Chem., Int. Ed.* **2013**, *52*, 8976−8969.
(84) Murray, K. K.; Lykke, K. R.; Lineberger, W. C. Spectroscopy and Autodetachment Dynamics of PtN^-. *Phys. Rev. A: At., Mol., Opt. Phys.* **1987**, *36*, 699.
(85) Lykke, K. R.; Neumark, D. M.; Andersen, T.; Trapa, V. J.; Lineberger, W. C. Autodetachment Spectroscopy and Dynamics of $CH_2CN^-$and CD_2CN^-. *J. Chem. Phys.* **1987**, *87*, 6842.
(86) Marks, J.; Brauman, J. I.; Mead, R. D.; Lykke, K. R.; Lineberger, W. C. Spectroscopy and Dynamics of the Dipole-Supported State of the Acetyl Fluoride Enolate Anion. *J. Chem. Phys.* **1988**, *88*, 6785.
(87) Yokoyama, K.; Leach, G. W.; Kim, J. B.; Lineberger, W. C. Autodetachment Spectroscopy and Dynamics of Vibrationally Excited Dipole-Bound States of $H2CCC^-$. *J. Chem. Phys.* **1996**, *105*, 10706.
(88) Dobulis, M. A.; Thompson, M. C.; Patros, K. M.; Sommerfeld, T.; Jarrold, C. C. Emerging Nonvalence Anion States of [Isoprene - H] · H_2O Accessed via Detachment of OH^-· Isoprene. *J. Phys. Chem. A* **2020**, *124*, 2279−2287.
(89) Anstöter, C. S.; Verlet, J. R. R. Gas-Phase Synthesis and Characterization of the Methyl-2,2-dicyanoacetate Anion Using Photoelectron Imaging and Dipole-Bound State Autodetachment. *J. Phys. Chem. Lett.* **2020**, *11*, 6456−6462.
(90) Bull, J. N.; West, C. W.; Verlet, J. R. R. Internal Conversion Outcompetes Autodetachment from Resonances in the Deprotonated Tetracene Anion Continuum. *Phys. Chem. Chem. Phys.* **2015**, *17*, 32464−32471.
(91) West, C. W.; Hudson, A. S.; Cobb, S. L.; Verlet, J. R. R. Communication: Autodetachment versus Internal Conversion from the S_1 State of the Isolated GFP Chromophore Anion. *J. Chem. Phys.* **2013**, *139*, 071104.
(92) Computational Chemistry Comparison and Benchmark DataBase Release 21, August 2021, *Standard Reference Database 101, National Institute of Standars and Technology*. https://cccbdb.nist.gov/exp2x.asp?casno=107222&charge=0#1998Kuc.
(93) Durig, J. R.; Tong, C. C.; Li, Y. S. Microwave Spectrum of cis-Glyoxal. *J. Chem. Phys.* **1972**, *57*, 4425−4427.
(94) Hammer, N. I.; Diri, K.; Jordan, K. D.; Desfrancois, C.; Compton, R. N. Dipole-Bound Anions of Carbonyl, Nitrile, and Sulfoxide Containing Molecules. *J. Chem. Phys.* **2003**, *119*, 3650−3660.
(95) Jordan, K. D.; Wang, F. Theory of Dipole-Bound Anions. *Annu. Rev. Phys. Chem.* **2003**, *54*, 367−396.
(96) Paldus, J.; Ramsay, D. A. The 4550 Å Band System of Glyoxal. I. Rotational Analyses of the (0−0) bands for C2H2O2, C2HDO2, and C2D2O2. *Can. J. Phys.* **1967**, *45*, 1389−1412.
(97) Compton, R. N.; Bouby, L. Formation d'IonsNegatifsdan le Glyoxalet le Diactyle. *Compt. Rend. Acad. Sci. (Paris)* **1967**, *264C*, 1153−1156.

https://doi.org/10.1021/acs.jpca.1c07163
J. Phys. Chem. A 2021, 125, 9128−9142

(98) Hirata, K.; Kim, K.; Nakamura, K.; Kitazawa, H.; Hayashi, S.; Koyasu, K.; Tsukuda, T. Photoinduced Thermionic Emission from $[M25(SR)18]^{-\cdot}$ (M = Au, Ag) Revealed by Anion Photoelectron Spectroscopy. *J. Phys. Chem. C* **2019**, *123*, 13174−13179.
(99) Görling, Ch.; Jalviste, E.; Ohta, N.; Ottinger, Ch. Lifetime Measurements of the Collision-Free Slow Fluorescence from Glyoxal S_1/T1 Gateway Levels in a Beam. *J. Phys. Chem. A* **1998**, *102*, 10620−10629.
(100) Scheer, A. M.; Aflatooni, K.; Gallup, G. A.; Burrow, P. D. Bond Breaking and Temporary Anion States in Uracil and Halouracils: Implications for the DNA Bases. *Phys. Rev. Lett.* **2004**, *92*, 068102.
(101) Chernyshova, I. V.; Kontrosh, E. E.; Shpenik, O. B. Collisions of Slow Electrons with Thymine Molecules. *Opt. Spectrosc.* **2018**, *125*, 845−852.
(102) Boudaiffa, B. Resonant Formation of DNA Strand Breaks by Low-Energy (3−20 eV) Electrons. *Science* **2000**, *287*, 1658.
(103) Dugal, P.-C.; Abdoul-Carime, H.; Sanche, L. Mechanisms for Low-Energy (0.5−30 eV) Electron-Induced Pyrimidine Ring Fragmentation within Thymine- and Halogen-Substituted Single Strands of DNA. *J. Phys. Chem. B* **2000**, *104*, 5610−5617.
(104) Huels, M. A.; Boudaiffa, B.; Cloutier, P.; Hunting, D.; Sanche, L. Single, Double, and Multiple Double Strand Breaks Induced in DNA by 3−100 eV Electrons. *J. Am. Chem. Soc.* **2003**, *125*, 4467−4477.
(105) Sarre, P. J. The Diffuse Interstellar Bands: A Dipole-Bound State Hypothesis. Mon. *Mon. Not. R. Astron. Soc.* **2000**, *313*, L14−L16.
(106) Larsson, M.; Geppert, W. W.; Nyman, G. Ion Chemistry in Space. *Rep. Prog. Phys.* **2012**, *75*, 066901.

https://doi.org/10.1021/acs.jpca.1c07163
J. Phys. Chem. A 2021, 125, 9128−9142